Applied Geochemistry 136 (2022) 105166

Contents lists available at ScienceDirect

Applied Geochemistry

journal homepage: www.elsevier.com/locate/apgeochem

Dynamics of natural discharge of the hydrothermal system and geyser eruption regime in the Valley of Geysers, Kamchatka

A.V. Kiryukhin [a,b,*], A.Y. Polyakov [a], N.B. Zhuravlev [a], N. Tsuchiya [c], T.V. Rychkova [a], O. O. Usacheva [a], I.K. Dubrovskaya [a]

[a] Institute of Volcanology & Seismology FEB RAS, Piip 9, Petropavlovsk-Kamchatsky, 683006, Russia
[b] Kronotsky Federal Nature Biosphere Reserve, Ryabikova 48, Elizovo, 684000, Russia
[c] Graduate School of Environmental Studies, Geomaterial and Energy Lab., Tohoku University, Sendai, 980-8579, Japan

ARTICLE INFO

Editorial handling by Dr. Z Zimeng Wang

ABSTRACT

The total deep component natural mass discharge Q_d (defined in terms of chloride mass discharge Q_{cl}) of the Valley of Geysers, on an average ranges from 280 kg/s from 1961 to 1984, to 230 kg/s after 2015. Post 2012, discharge measurements reveal a seasonal variation: the discharge increases (340–370 kg/s) during the winter-frozen period, and decreases during the summer flooding period (≈100 kg/s). Long term annually averaged Q_d is 274 kg/s, Q_{cl} is 0.247 kg/s and heat flow is 265 MW. In the course of using high-frequency (min^{-1}) observations specific conductance measurements from 2017 to 2020, the total natural discharge was found to be cycling due to the internal cycling of geysers. It was mostly sensitive to the Bolshoy and Velikan geysers with averaged intervals between eruptions of 60 min and 70 min, respectively. The tracer chloride method estimates the volume of hot water erupted from geysers. This method yielded the following estimates: 5–34 m^3 of hot water cyclically erupted from the Bolshoy geyser; 0.5–4.5 m^3 erupted from the Velikan geyser between 2018 and 2020, and 24–144 m^3 erupted before the 2014 mud-flow disaster; and 289–330 m^3 erupted from the Grot geyser between May–June 2012. The seasonal features of natural discharge mentioned above may be explained in terms of cold-water infiltration into a two-phase geyser geothermal reservoir, especially if gas-phase condensation induces vacuum conditions, which may further reduce some thermal discharge features.

1. Introduction

Valley of Geysers is one of a few places in the world, where abundant geysers activity took place, attracting more than 6000 visitors annually (mostly during time period from July to September). Discovered in 1941 by Tatiana Ustinova as a Kingdom of Geysers, this place was eventually become a source of catastrophic disasters, including 20 mln m^3 landslide on June 3, 2007 (triggered by hydrothermal explosion (Kiryukhin et al., 2012)) and 3 mln m^3 mudflow on January 3, 2014 (triggered by sliding of Uson caldera rim rocks, apparently caused by magmatic activity of Kihpinych volcano). Its lucky, that nobody damaged at this times. Danger of being on the foothills of Kihpinych volcano, seems to be related with its magma activity. Hence, a proper monitoring set of hydrothermal system discharge and geysers activity (cycling timing and volumes of eruptions) is crucial to get a message on forthcoming geological disasters.

The thermal water recharge of high-temperature hydrothermal systems Q_{upflow} is traced on the surface by deep-component water discharge Q_d (Fig. 1). Q_{upflow} may be estimated only through Qd measurements at the surface using chloride mass flow rate Qcl, as chloride is a stable tracer of deep-component water recharge. While Q_{upflow} is rather stable due to large volume of hydrothermal system as a whole and a long passway from regional recharge to local discharge area, Q_d is sensitive to changes in local hydrology and meteorological conditions, which form an outflow boundary condition. Thus, another issue is how such powerful hydrothermal system responds to top boundary conditions (BC) change caused by flooding (due to landslides damming or seasonal snow melting) or caprock erosion (made by mudflows). Worth noting some examples of such significant top BC driven changes in two-phase reservoirs: (1) Liquid water inflows in production CO_2-rich hydrothermal reservoirs either kill them (Ohaaki, New Zealand (Daysh et al., 2020)) or add deliverability (Geysers, USA (ROBERTSON-TAIT et al., 2021)); (2) Dry periods may empty geysers (Hurwitz et al., 2020), while flooding ceased its too (Kiryukhin et al., 2012); (3) Shallow water

* Corresponding author. Institute of Volcanology & Seismology FEB RAS, Piip 9, Petropavlovsk-Kamchatsky, 683006, Russia.
E-mail address: AVKiryukhin2@mail.ru (A.V. Kiryukhin).

https://doi.org/10.1016/j.apgeochem.2021.105166
Received 16 September 2021; Received in revised form 5 December 2021; Accepted 6 December 2021
Available online 10 December 2021

level reservoirs may switch to steam flash and hydrothermal explosions, while less water reservoirs keeping steam jets in secure conditions (Brown and Lawless, 1998).

The objectives of the present study focuses on the Valley of Geysers hydrothermal system, which has the largest deep thermal water outflow observed in Kamchatka, Russia, to measure and estimate long term year trends and seasonality of Qd, deep thermal water component discharge, and geysers erupted volumes using tracer chloride method.

2. Antecedents about chloride inventory method

The chloride mass flowrate (Q_{cl}) has been used to estimate Q_d in volcanic environments, as applied in New Zealand by Ellis and Wilson (1955). Qd was also estimated by V.V. Aver'ev in May 1958 (in the low water period) for thermal waters of the Pauzhetsky geothermal field in Kamchatka, using the chloride method by Averiev and Sugrobova (1965). For this purpose, the chloride-ion inflow rate into the Pauzhetsky River from the thermal site through which the river flowed, was estimated. This was based on hydrometric measurements and chemical sampling upstream and downstream of the thermal water discharge area. The Qcl that the Pauzhetka River receives as it flows past the thermal site was estimated to be 0.1497 kg/s. Furthermore, taking the parental mass fraction of chloride ion C_{upflow} in the thermal water equal to $1.58 \cdot 10^{-3}$, the deep thermal Qd component was estimated as, $Q_d = Q_{cl}/C_{upflow}$, that is equal to 95 kg/s.

The Yellowstone National Park (YNP) magmatic hydrothermal system is the most known example in relation to this study. The estimation of the deep component of thermal Q_d in the YNP was pioneered by R. Fournier (1989). A great description of the Cl inventory was also given by Ingebritsen et al., (2001).

In this paper, to estimate the total mass discharge of the deep component of thermal water (Q_d, kg/s), the mass rate of discharge of the river (Q_r, kg/s), and the Cl mass fraction (kg/kg) carried by the river waters (C_r) were utilized (in SI units). We keep here SI units to maintain compatibility chloride tracer models, which are widely used for non-isothermal multiphase-multicomponent ground flows TOUGH2-modeling (Pruess et al., 1999).

For this purposes let's consider water and tracer (Cl) mass balances in a single river basin with a single group discharge (so called lamped-parameter model). Water mass balance is:

$$Q_r = Q_d + Q_{upstream} \quad (1)$$

-where, $Q_{upstream}$ is river upstream mass discharge. Tracer mass balance is:

$$C_r \cdot Q_r = C_{upflow} \cdot Q_d + C_b \cdot Q_{upstream} \quad (2)$$

-where, C_r is the mass fraction of chloride in the river, C_{upflow} is the Cl mass fraction of deep water from the hydrothermal system (parental thermal fluid) was suggested to be the maximum before dilution (Fig. 1), C_b is the background mass fraction of Cl in the meteoric waters.

Substituting $Q_{upstream}$ from (1) to (2), Q_d deduce:

$$Q_d = Q_r \cdot (C_r - C_b)/(C_{upflow} - C_b) \quad (3)$$

Further, taking in account that Cl mass rate in the river associated with the deep component is $Q_{cl} = C_{upflow} \cdot Q_d$, coming to:

$$Q_{cl} = C_r \cdot Q_r - C_b \cdot (Q_r - Q_d) = Q_r \cdot (C_r - C_b) + Q_d \cdot C_b \quad (4)$$

Equations (3) and (4) can be further simplified neglecting C_b:

$$Q_d = Q_r \cdot C_r / C_{upflow} \quad (5)$$

$$Q_{cl} = Q_r \cdot C_r \quad (6)$$

A convective heat recharge CHF may be also derived from Eq. (5):

$$CHF = h_d \cdot Q_d \quad (7)$$

- where h_d is a deep upflow fluid enthalpy. If single phase conditions prevail in a deep part of reservoir, then water enthalpy h_w may be substitute h_d and water chemical geothermometers may be used for deep reservoir temperature T estimates. Subsequently h_w is defined as a function of T, and CHF may be expressed in a form of:

$$CHF = h_w(T) \cdot Q_d \quad (8)$$

Mass balance definition from Eq. (3) in this paper is analog volume balance definition from Eq. (1) (Ingebritsen et al., 2001), and convective heat recharge CHF from Eq. (8) in this paper is analog advective heat transport by hot spring system from Eq. (3) (Ingebritsen et al., 2001). In latter paper is also mentioned low values of C_b (from 0.2 to 0.7 ppm) were observed in Oregon Cascade Ranges and Yellowstone sites "background chloride values", that is assumed to be a sum of weathering (0.7 ppm) and precipitation (0.2 ppm) substitutes (Norton and Friedman, 1991). In Geysernaya river "background chloride values" are generally less than 2 ppm (mass fraction of $2 \cdot 10^{-6}$) (upstream of Chloridny boiling spring #54, Fig. 1).

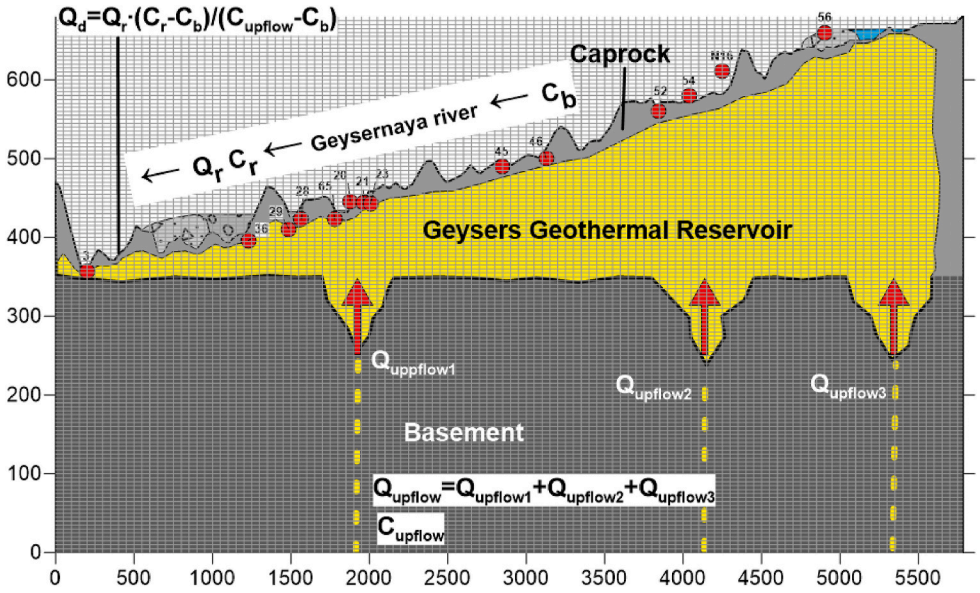

Fig. 1. Conceptual model for tracer chloride method application for deep thermal water component discharge estimation (modified from Kiryukhin et al. (2018). Q_{upflow} – deep thermal water upflow mass rate, C_{upflow} – deep thermal water chloride mass fraction (parental thermal fluid), Q_r –river discharge (mass rate), Cr – river chloride mass fraction, C_b – background chloride mass fraction, Q_d – deep thermal water component mass discharge. Notes: (1) Numbers above the thermal features, shown by filled red circles, correspond to Table 3 (Kiryukhin et al., 2011), (2) Axes scales are given in meters. (For interpretation of the references to color in this figure legend, the reader is referred to the Web version of this article.)

This tracer chloride method also automatically compensates for the boiling and mixing of the rising thermal waters. The R. Fournier estimates noted in Yellowstone was 3000 kg/s, and varied by 25–50% within a "hydrologic year cycle" (note hydrological year cycle is defined here on one year duration time interval from current time (days counted from January 01, 1900) as mod (current time, 365.25). Further, he also noted that the uncertainty of estimating the hidden thermal water discharge may reach 20–30%. In addition, discharge also depends on seismicity, which favors the infiltration of meteoric waters into the underlying magma system (Fournier, 1989).

The classical Cl method requires chloride concentrations and flow-rate data, which are obtained using a discreet set of synchronized chemical sampling and hydrometric measurements. This limits the frequency and volume of the Q_d estimations.

The next era of the deep component of thermal water discharge Q_d estimates arrived with loggers of conductance and automated acoustic Doppler flowmeters, with a strong correlation observed between YNP river water conductance and Cl concentrations (McCleskey et al., 2012; 2016, 2019). Using the discrete flow rate data of the river and the same Cond-Cl correlation, one can calculate the chloride mass rate Q_{cl} (Eqs. (4) and (6)).

This assisted to obtain more frequent measurement sets and understand the seasonal trends of Q_d in YNP in the following ways: (1) Big Yellowstone rivers display Cl run off increase during snow melting (Friedman and Norton, 2007, McCleskey et al., 2012), which is explained by Cl accumulation in YNP lakes during winter; (2) the Firehole River, which drains near the Upper Geyser Basin (Q_d was estimated there from 1200 to 1400 kg/s, or almost half of the YNP), is exhibiting an exceptional rate of Cl decline during the flooding time period (Fig. 12C in McCleskey et al., 2012). In terms of Q_d, the thermal water discharge of the upper Geysers Basin decreases during the flooding time period.

The Geysernaya River in the Valley of Geysers, Kamchatka (Fig. 2) has some common features with the Firehole River in the YNP: a relatively narrow basin, a high concentration of geysers and hot springs in a small area, similar flowrates, and a large deep component thermal Q_d (estimated between 220 and 370 kg/s; Sugrobov et al., 2009; Kiryukhin et al., 2018). Hydrometric measurements conducted between 2007 and 2009 in section #3 (Dam section, Fig. 2) exhibit the river Q_r amounting to 1200 kg/s in April–May, (low water period), and 2800–3600 kg/s in July (early post-flooding period), and 1700–3100 kg/s (September–October; Kiryukhin et al., 2012). Thus, this is a typical case study to analyze the type of time-dependent outflow conditions that operate here.

However, that field surveys are difficult in the Valley of Geysers (Fig. 2) as the conditions are considerably adverse compared to the YNP: (1) No road access, the only way to reach some features is by a helicopter

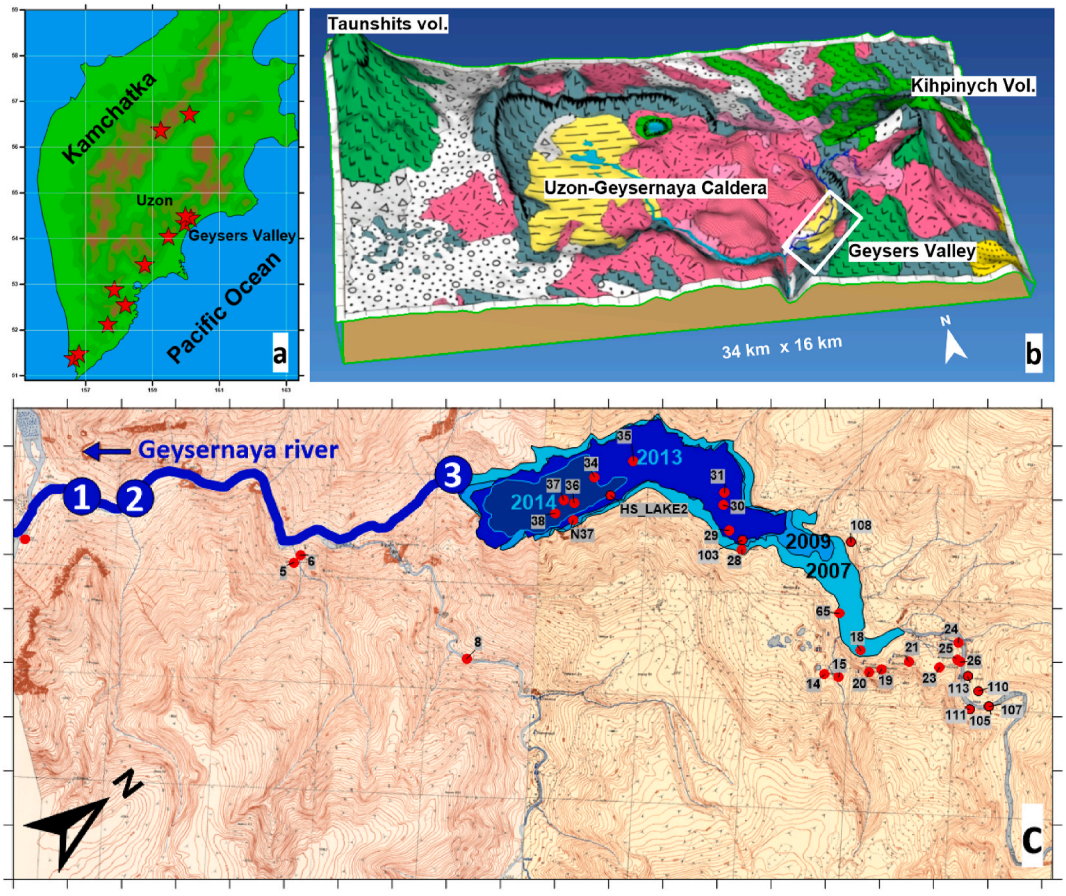

Fig. 2. Kamchatka high temperature geothermal systems shown by red stars (upper left, Figure a) and schematic 3D view of the Uzon–Geysernaya caldera (upper right, Figure b). The geological units are displayed in different colors: alluvial and glacial deposits (light gray), caldera lake deposits (Q_3^4) (yellow), rhyolite–dacite extrusions (ξQ_3^4 and $\alpha\xi Q_3^4$) (pink), pre-caldera tuffs and sedimentary deposits (gray), and basalt–andesite lavas (green) (αQ_3^{1-2}, αQ_3^3, and Q_3^3 ust), Axes scaling 1 km. (For interpretation of the references to color in this figure legend, the reader is referred to the Web version of this article.) Lower figure (c): local topographic map of the Lower Geysers Basin, Valley of Geysers (Kamchatka) with positioning of the main geysers and boiling springs. #28 – Bolshoy Geyser, #23 – Velikan Geyser, #20 – Grot Geyser, other numbers correspond to the table 5 (Kiryukhin, 2016) or table (Kiryukhin, 2020, Appendix 6-A, Table 6-A.1), where current modes of thermal features is defined too. Points/sections of measurements (1, 2, and 3) are shown by blue circles with numbers. The distribution of Podprudnoye Lake in 2007, 2009, 2013, and 2014 is shown in different colors with corresponding marks. Note: The extended geological map of the Valley of Geysers is shown in (Fig. 2 in Kiryukhin, 2016). Axes scaling is 100 m. Note: geological map of Valley of Geysers is presented in Kiryukhin, 2016, Fig. 2.

only; (2) Moreover, a small helicopter is required to visit measurement points in winter–spring; (3) No bridges in the Geysernaya river restrict visiting of the right bank below the junction with the Shumnaya river; (4) Frequent "small" mudflows in late autumn and summer flooding periods run along the Geysernaya river which has destroyed and/or removed the equipment which was installed for long-term observations (2013, 2015, 2016, 2017, 2018).

3. Methods of measurements and analysis

3.1. Measurements of interval between geysers eruptions

HOBO U12-015 temperature loggers (measurement range: 40° to 125 °C, accuracy: ± 0.25 °C from 0° to 50 °C, resolution: 0.03 °C at 25 °C, response time in water <3.5 min, typical to 90%) were used to measure the interval between geysers eruptions (IBE) of the Velikan and Bolshoy Geysers, starting in July 2007 and are currently ongoing. The loggers, which were installed in the channels of water discharge from the geysers, recorded the temperature of the water outflow every 5 min. The eruption time of the geysers was estimated according to the time of the absolute maximum temperature prior to its absolute minimum (in a cycle). Velikan and Bolshoy are the most powerful and spectacular geysers in the Valley of Geysers (Kiryukhin et al., 2012). Thus, they were selected to monitor the cycling and hydrochemical regimes.

3.2. Geysernaya river flowrate, chloride and deep hydrothermal discharge measurements and estimations

The Mainstream 400P Doppler flowmeter was used since 2016 to measure and records flows for Geysernaya river (for short term tests, referenced as tests #1 - #7 in Section 5.1). The Mainstream embeds a CPU (Central Processing Unit - analog-to-digit transformer), a level sensor, which is measured using a piezo-resistive sensor (accuracy of 0.7 cm). The velocity is measured by a Doppler-effect velocity sensor. The Mainstream velocity sensor transmits ultrasonic signals in the fluid in order to create a wide inspection and measurement area. Particles and air bubbles suspended in fluid in the inspection area reflect the ultrasonic signal that goes back to the sensor. The Mainstream measures the actual mean velocity (accuracy of 1 cm/s, range from 1 cm/s to 5 m/s). During measurements, Mainstream 400P was instructed to measure and calculate average velocity in a cross-sectional rectangle of h x L, where h – is stream width (was assigned to 3.5 m as average effective Geysernaya river width), L – is a water level in a stream (which Mainstream measure itself). In case of actual h was not equal to 3.5 m, a coefficient h/3.5 was applied to Mainstream 400P flowrate estimates.

Before 2016, a hydrometric vane GR-55 was used. In that case flow velocities were measured in a points of 0.5 m apart each other across the river at a depth of 0.5 L, then river flowrate was integrated using standard hydrometric routine.

In addition, for long term tests only, mentioned as tests #LT1 and #LT2 in Section 5.2, a pair of HOBO U20-001-01 loggers (operation range from 0 to 207 kPa or approximately 0–9 m of water depth; factory calibrated range from 69 to 145 kPa, 0° to 40 °C; water level accuracy 0.5 cm (typical), 1.0 cm (maximum); resolution <0.21 cm water; pressure response time (90%)<1 s) with set interval measurements of 10–20 min was used to log the Geysernaya River level. One logger recorded the barometric pressure, and the other was installed in the river to record the total pressure of the water column and atmospheric pressure. The water level of the river was determined by the difference between the pressure records of the two loggers. A linear rate-level formula to determine the flowrate of the river by the water level was calibrated according to the results of flowrate measurements using either direct measurements of flow velocity (by hydrometric vane GR-55, test #LT1) and cross-sectional area of the river, or Mainstream 400P flowmeter measurements (test #LT2) (estimated accuracy of linear rate-level formula is 42 kg/s). Note, that use of rate-level curves for long term tests was implemented to avoid mud-flow loss of flowmeter (that is much more expansive compare to other instruments used).

The deep component discharge of thermal water was estimated by the chloride method at observation cross-sections #1 and #2 at the mouth of the Geysernaya River, and in cross-section #3 (dam point) at the mouth of Podprudnoye Lake (2008–2012) (Fig. 2). A HOBO U24-001 logger (low range of 0–1,000 μS/cm with a set recording interval of 0.5–20 min) was used to continuously record the solution specific conductance.

Solution specific conductance enabled the simultaneous assessment of changes in chloride ion concentration in the Geysernaya River. Conversion of solution specific electro conductance into chloride concentration was performed using planar regression of direct sampling data (10 points, STD = 8.9 ppm) in observational cross-sections #1 and #2, obtained during 2017–2020 year time period (Appendix 2):

$$C = -3.461*T + 0.254 * SC + 31.451 + 0.1634 * Time \quad (9)$$

where, C is the chloride concentration (ppm), T is the temperature (°C); SC is the specific electrical conductance (μS/cm), and Time is the time difference between the time of logger installation and the time of measurement, days. Time measurement corrections accounted for logger fouling were applied only for long-term monthly measurements.

Seven short-term tests (from 21 min to 61 h) in sections #1 or #2 of the Geysernaya River were conducted with recording frequency from 1 to 2 min^{-1}, two long term tests (from 108 to 126 days) in sections #1 or #3 of the Geysernaya River (Fig. 2, Appendix, Photo 6) were conducted with recording frequency from 0.05 to 0.1 min^{-1}, a water samples were collected at the start and end times of each tests for chemical analysis and subsequent SC/Cl calibration. Finally, the obtained specific conductance values were converted into Cl concentrations using Eq. (9).

To estimate the total discharge of the deep component of thermal water (Q_d, kg/s), the Cl method (Eq. (5), see above) was applied to the tests observational data. The Cl concentration of deep water from the hydrothermal system (parental thermal fluid, C_{upflow}, Fig. 1) was assigned to be the maximum before dilution at 900 ppm (Sugrobov et al., 2009).

3.3. A simple theory of tracer tests applied for estimations of geyser discharges in a river

An interesting feature revealed in the Valley of Geysers during high-frequency conductance-flowrate measurements (from 1 to 2 records per min) is cycling with an interval of approximately 1 h. A closer look at this cycling reveals (see below) that, large maxima of Cl cycles correspond to Bolshoy Geyser eruptions, and small maxima correspond to Velikan geyser eruptions.

Short-term cycling data can be used to estimate the volumes of subsequent Bolshoy and Velikan geyser eruptions using simple relationships developed for tracer tests (Fig. 3, see also Moore, 2005). Tracer tests are useful tools to estimate traceable (chloride ion) mass M injected (erupted from geyser) into the river, if river flow rate Q_r and time-dependent tracer (chloride ion) concentrations in river C(t) during tracer travel time interval [t1,t2] are known:

$$M = Qr \cdot \int_{t1}^{t2} C(t)dt \quad (10)$$

In Eq. (10) $C(t) = C_r(t) - C_b(t)$ is the cycling component of discharge, which is the difference between $C_r(t)$ (tracer concentration in a river) and $C_b(t)$ (background trend of tracer concentration in a river) (see Fig. 3). By estimating the traceable (chloride ion) mass erupted from a specific geyser, we can also estimate V, volume of the thermal water erupted from a specific geyser, if the tracer (chloride ion) concentration in a geyser, C_g is known. In this study, chloride concentration was used as a tracer; thus:

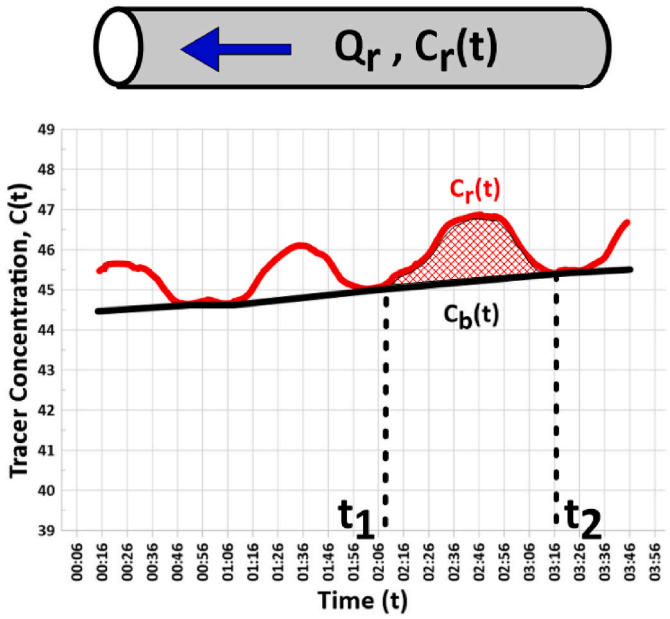

Fig. 3. Explanation picture: how to measure mass (M) of a tracer erupted in the river using Eq. (10). Legend: Q_r – rate of the river, $C_r(t)$ – tracer concentration in a river, $C_b(t)$ – background trend of tracer concentration in a river, t – time, The cross-hatched area is equal to $\int C(t)dt$, chloride ion is the tracer.

$$V = M/C_g \quad (11)$$

-where, M is the chloride mass erupted from the geyser and C_g is the chloride concentration in a specific geyser.

Error propagation analysis for Eqs. (5), (9)–(11) shows the following. If Q_d was estimated from Eq. (5), then relative Q_d error is a sum of relative errors of Q_r, C_r-C_b and C_{upflow}, that are 5% (Hurwitz et al., 2007), 9% (Table A2-1, Fig. A2-1) and 2% (Analytical Error) correspondingly. Hence sum Q_d error is 16%. Note according to McCleskey et al. (2012), the chloride mass flow rate calculation error is ±7%. Regarding Eq. (10): Q_r error is 5% (as mentioned above), integral error is 9%, then M error is a sum, that is equal to 14%. Now coming to erupted geysers volumes estimations of Eq. (11): M error is 14% (see above), C_g geyser chloride concentration error may be either 2% (Analytical Error, if we use actual geyser eruption data) or 6%–7% (STD for transient C_g Velikan&Bolshoy geysers during last 10 years (see Fig. 10 A in Kiryukhin et al., 2018, Fig. 6.10 in Kiryukhin, 2020). Thus sum error of V is in a range from 16% to 21%.

4. Review of cyclic regime of geysers Bolshoy and Velikan

Velikan and Bolshoy Geysers are the most regular and impressive geysers in the Valley of Geysers (Appendix, Photos 1 and 2), so they were chosen for regular monitoring for cycling. Sections 4.1 and 4.2 (except of last paragraph and Fig. 4) are briefly summarized a previously published results (Kiryukhin, 2016; Kiryukhin et al., 2018), while the rest (Section 4.3) is a new one.

4.1. Bolshoy Geyser (before 2015)

Before 2007, according to measurements from August to October 2003, the average IBE of the Bolshoy Geyser was 108 min (1.8 h) (according to Droznin, 2007 (pers. com); see also Fig. 8 b in Kiryukhin et al., 2018). Observations from 2008 to 2014, (after the 2007 landslide) showed that the operating mode of the Bolshoy Geyser was most sensitive to the level of Lake Podprudnoe. The Bolshoy Geyser stopped erupting when the lake level exceeded the level of the lower edge of the geyser conduit, and cold water from the lake penetrated the geyser channel (June 2010). When the lake level dropped below the conduit entry level (25–30 cm), the Bolshoy Geyser started erupting again (IBE from 45 to 85 min on average). In addition, observations in 2011–2013 also found that Bolshoy Geyser eruptions stopped during the spring–summer floods (June 18–July 9, 2011, June 22–24, and July 2–3, 2012; June 5–July 10, 2013) and during an autumn typhoon flood (October 18–20, 2013). At this time, the lake level was below the conduit entry edge, so the eruption stops are probably indicative of a breach of the geyser cone wall seal during periods of flood rise. The average IBE of the Bolshoy Geyser during the period of observation from 2007 to 2013 was 63 min; 19,712 eruptions of the geyser were recorded; the IBEs were normally distributed, with a standard deviation of 7 min. As a rule, the height of the Bolshoy Geyser eruptions reached 5–8 m, and the duration of eruptions was 2–3 min. The Bolshoy Geyser was the only "time-keeper" of the catastrophic mudflow flow in January 2014. The records of the temperature logger installed on the Bolshoy Geyser indicates the exact time of mud flow pouring into the geyser channel: ~23:00 (local time) on January 03, 2014. At this point, the IBE dramatically decreased from 60 to 30 min. Over the next few months, the IBE slowly increased and was 44 min on September 06, 2014. No obvious visual decrease in the Bolshoy Geyser eruption power was observed after the 2014 mudflow.

4.2. Velikan Geyser (before 2015)

The first discrete observations in the period 1941–1991 showed that the IBE of the Velikan Geyser slowly increased from 180 to 400 min (see also Fig. 8 a in Kiryukhin et al., 2018). According to 1991–2004 measurements, on the eve of the catastrophic landslide in 2007, the average IBE of the Velikan Geyser was 375–379 min (Droznin, 2007, pers. com.). The geyser IBE history for the period 1941–2007 is characterized by a nearly linear increasing trend (+200 min for 65 years, or +3 min/year) with the geyser channel geometry remaining unchanged. In this case, the duration of Velikan's "vitality" until 2004 can be estimated to be about 120 years. But, non-linear IBE vs time models are not excluded too. From July 2007 to September 2013, the average IBE of the Velikan Geyser was 340 min, based on 8216 recorded eruptions. IBE was characterized by a normal distribution with a standard deviation of 52 min.

After the catastrophic landslide in 2007, the IBE exhibited a tendency to stabilize after declining for the first three years: 379 (2007), 359 (2008), 323 (2009), 334 (2010), 337 (2011), 337 (2012), and 334 (2013) min. The IBE of the Velikan geyser depends on the amount of precipitation that falls directly into the geyser's pool. Heavy snowfalls and typhoons can delay the onset of eruptions and lead to increased IBE. The maximum observed IBE was 32 h during heavy snowfall on February 29, 2008 (Kiryukhin, 2016, sec. 3.3.1).

Anomalous increase in the IBE of the geyser correspond to the winter seasons from 2007 to 2013. This indicates the seasonal dependence of the IBE of the Velikan Geyser on the discharge boundary conditions. The graph of changes in the IBE of the Velikan Geyser within the hydrological cycle from January to December for the entire observation period from 2007 to 2013 displays the occurrence of an anomalous IBE increase over 600 min and decrease below 200 min only in winter. Thus, it demonstrates a pronounced seasonal character. In winter, the IBE increases by an average of 41 min compared to summer (Fig. 7 in Kiryukhin, 2016).

Mud flow on, January 03, 2014, significantly damaged the Velikan Geyser (Appendix, Photo 3). Temperature loggers were carried away by debris flow. Thus, no data was recorded on geyser cycling from September 2013 to April 2014. In April 2014, the geyser cycling monitoring system was restored, and the IBE of the Velikan Geyser was observed to be 90 min. The geyser pool was cut by the mudflow by approximately 0.3 m, the basin area decreased from 12.2 to 5.5 m^2 (Fig. 4), the geyser channel was partially filled with mudflow deposits, while the conduit zond-penetrating depth recovered to 5 m by 2017. The

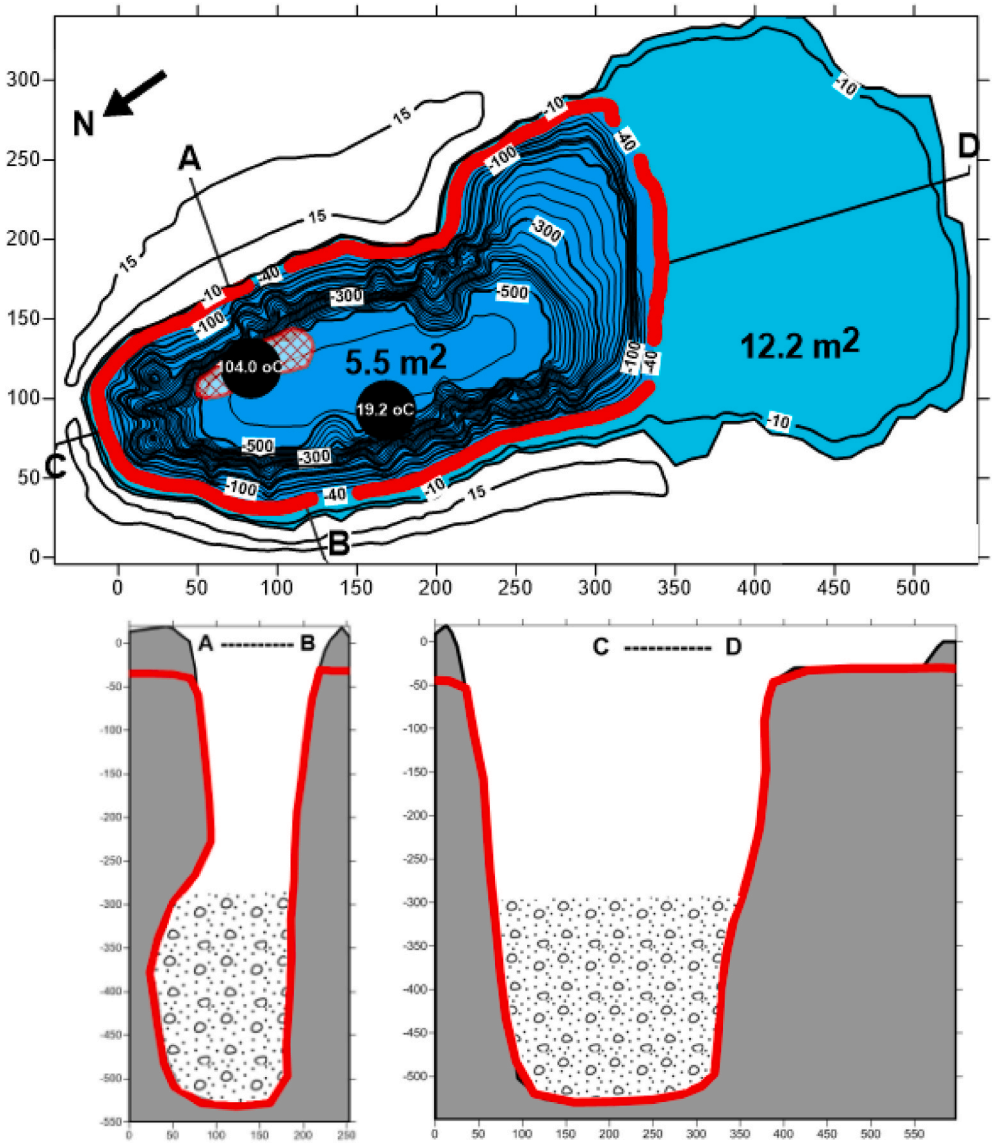

Fig. 4. Comparison of the Velikan Geyser conduit geometry after and before the mud flow of January 03, 2014. The contours of the new shape are shown in bold red line. Top panel is topography of the conduit. AB and CD are the vertical sections of the conduit, fill pattern in the bottom mean mudflow of January 03, 2014 debris. Black circles with temperature values corresponds to bottom measurements on 30–31.08.2017. Scale in cm. (For interpretation of the references to color in this figure legend, the reader is referred to the Web version of this article.)

eruptive power of the Velikan Geyser dropped significantly: the geyser's fountain height in 2014 decreased to 1–1.5 m compared to 15–20 m in the previous years. An interesting feature of the Velikan Geyser cycling since 2014 is the water level drawdown at 1.5 m below the ground surface after eruption. Indications for direct inflow of cold water from the Geysernaya River to the Velikan Geyser conduit bottom, as shown by temperature measurements in 2017, is displayed in Fig. 4. This may be explained by the cold water recharge from Geysernaya river, 30 m away from the Velikan Geyser (see Appendix, Photo 4).

4.3. Geysers cycling features in recent years (2016–2021)

The interval between eruptions (IBE) of the Bolshoy and Velikan geysers during the period from 2016 to 2021 (after catastrophic mudflow on January 03, 2014) are shown in Figs. 5 and 6 in terms of the hydrological year. The Bolshoy geyser erupted more frequently in winter, while the Velikan geyser runs more frequently in summer. Bolshoy is a cone-type geyser that protects itself from snow accumulation in winter, while Velikan is a pool type geyser that favors snow deposits. Thus, cooling due to winter snowfall delays the Velikan geyser IBE more than the Bolshoy geyser IBE. Hence, Bolshoy geyser (cone) and Velikan geyser (pool) act in a style of Old Faithful geyser (cone, is not modulated by precipitation) and Daisy geyser (pool, lengthen IBE's in a storm and cold weather conditions), described by Hurwitz et al. (2014). Interestingly, both geysers reached a close range of annually averaged IBE values in a range from 58 to 73 min after the catastrophic mudflow of January 03, 2014. Splitting of the Bolshoy geyser IBE (some eruptions missed) was recorded when Geysernaya river displayed closer to geyser conduit in 2017.

It is worth noting pressure rise seasonality in Geyserny Reservoir during flooding times. That is expressed in a form of new-born fountain phenomenon in the Valley of Geysers, which was first observed since its discovery in 1941. In the spring–summer flooding period, the rise in the water level of the Geysernaya River triggered new fountains of boiling water. This occurred on May 29, 2018, when a fountain of 1–1.5 m height suddenly started cycling in a river bottom near former Geyser #18 (Malahitovy Grot, sank in 2007; Fig. 2). This fountain terminated when the flooding period was complete. Another fountain was born on May 26, 2020, in place of the former boiling spring HS_Lake2 (Fig. 2, Appendix, Photo 5). A former hole on a slope, 2 m above the river level was used by boiling water to permanently blow out up to height of 3–7 m, at a zenith angle of 60°.

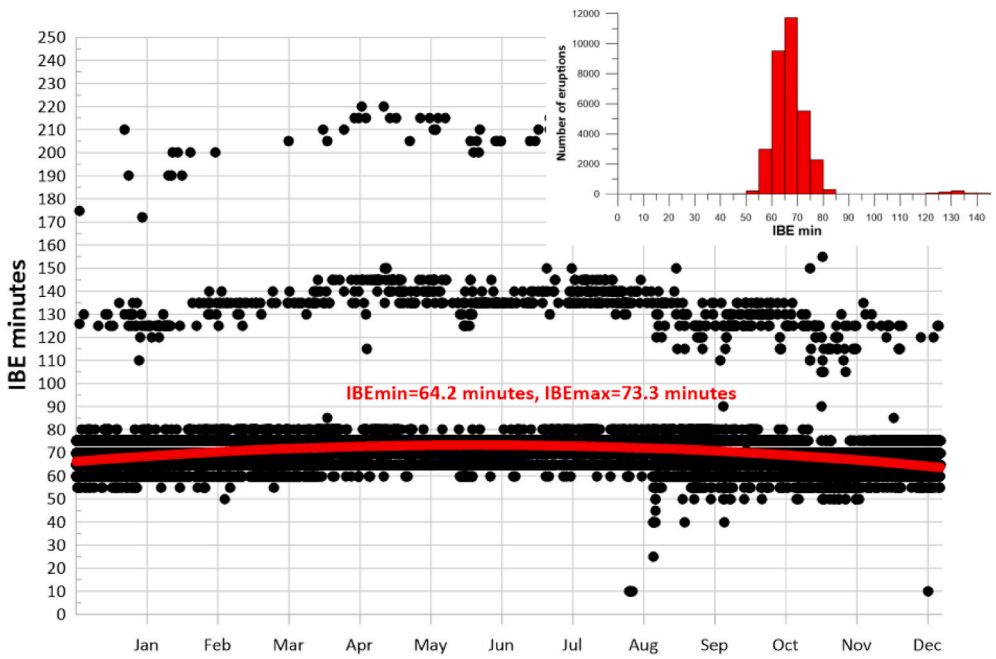

Fig. 5. Bolshoy Geyser IBE during hydrological year (data collected from 08.2016 to 04.2021). IBE min and IBE max are the min and max of the corresponding fitting curves (2-nd order polynoms were used.

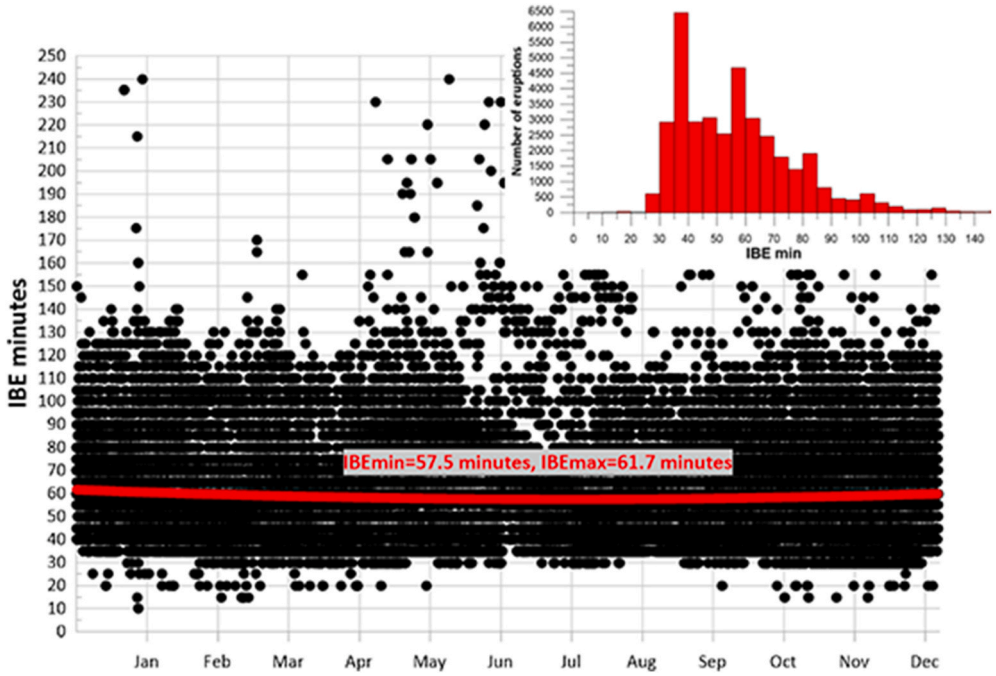

Fig. 6. Velikan Geyser IBE during hydrological year (data collected from 08.2016 to 04.2021). IBE min and IBE max are the min and max of the corresponding fitting curves (2-nd order polynoms were used.

5. Dynamics of the deep component water natural discharge of the Valley of Geysers hydrothermal system during the period between 2017 and 2020

5.1. Short term Q_d measurements (tests #1–7)

Short-term testing (from 21 min to 61 h) in sections #1 or #2 of the Geysernaya River (Fig. 2, Appendix, Photo 6) were aimed to estimate the short-term dynamics of the deep-component Q_d. The data (temperature and flowrate) and output results (Q_{cl} and Q_d estimates) for all tests are presented in Table 1.

Test #1 was conducted on December 24, 2017 in section #1 during a time period of 31 min (recording frequency was min^{-1}).

Test #2 was conducted on May 02, 2018 in section #1 during a time period of 21 min (recording frequency was min^{-1}).

Test #3 was conducted from August 29, 2018 to September 01, 2018 in section #2 of the Geysernaya River (Fig. 2) for 61 h (recording frequency was 0.5 min^{-1}).

In contrast to measurements performed in winter and spring (Tests #1 and #2), clear hour-cycling and day-cycling of observational

Table 1
Summary of short-term observations (tests #1-#7) of flowrates (Q_r), chloride content analytically defined in samples (C_r), temperature (T) in Geysernaya river during time period from 2017 to 2020 year. Q_{cl} is chloride mass rate, Q_d is deep component water discharge rate estimated using Eq. (5), $Q_{d\ av}$ is average for observational time period based on measured flowrates and chloride/specific electro-conductance values. Note 1: C_{upflow} (Fig. 1), was estimated to be the maximum before dilution at $0.9 \cdot 10^{-6}$ (or 900 ppm, Sugrobov et al., 2009). Note 2: Q_d standard error is assumed to be 16% (see section 3.3 above).

Test ##	Sec##	Date	Time	Duration	T, °C	C_r ppm	Q_r kg/s	Q_{cl} kg/s	Q_d kg/s	$Q_{d\ av}$ kg/s
1	1	24.12.17	13:08	31 min	18.3–18.9	130	2460	.320	356	350
2	1	02.05.18	11:32	21 min	25.7–25.8	170	1200	.203	226	235
3	2	29.08.18	18:39	61 h	12.8–17.5	43	2160	.093	103	104
3	2	01.09.18	7:59			39	1990	.078	86	
4	1	21.04.19	13:44	4.5 h	25.5–27.6	156	1800	.281	312	332
4	1	21.04.19	18:21			163	1900	.310	344	
5	1	30.08.19	19:30	38 h	20.5–24.6	63	2100	.133	148	161
5	1	01.09.19	8:45			71	2000	.142	158	
6	1	01.05.20	12:27	37 min	28.0–28.8	167	1190	.198	227	261
7	1	08.09.20	13:30	19 h	18.4–23.8	73	1020	.075	83	79
7	1	09.09.20	7:53			81	810	.066	73	

parameters were recorded (Fig. 7), which is related to the increase in test #3 duration. Very regular short-term variations (around 1-h) were detected in the Geysernaya River: 53 cycles over 61 h with a temperature rise of up to 0.4 °C and chloride maxima up to 8 ppm. Short-time Q_d variations are characterized by maxima of up to 6–10 kg/s.

The flowrate day-variations were ±150 kg/s in terms of running averaged (61). The chloride day-variations were ±3 ppm, and temperature day-variations were ±2 °C in the Geysernaya River. Day-time Q_d variations are characterized by night-time increases (up to 16 kg/s at 02:00–04:00) and day-time decrease (down to −16 kg/s at 12:00–18:00).

Some non-regular chloride variations of ±13–15 ppm were observed at different time intervals from 10 to 13 h, while no other parameter variations were clearly observed at that time.

Test #4 was conducted on April 21, 2019 in section #1 of the Geysernaya River (Fig. 2) for 4.5 h (recording frequency was min^{-1}). Due to the increase in the duration of the observations (compared to earlier winter-spring tests #1 and #2), we were able to see three small 6 ppm chloride peaks at 1.5 h apart.

Test #5 was conducted from August 30, 2019 to September 01, 2019 in section #1 of the Geysernaya River (Fig. 2) for 38 h (recording frequency was min^{-1}).

Clear hour-cycling of observational parameters was recorded, while no clear trend of day-cycling was observed (Fig. 8). Very regular short-term variations are represented by 31 cycles during 38 h with temperature local maxima of up to 0.4–0.6 °C and chloride local maxima up to 6–8 ppm. Q_d seems to records 12–16 kg/s local maximums synchronized with T and Cl short-time local maximums.

Temperature day-variations were ±2 °C in the Geysernaya River. In contrast to test #3, long-term Q_d variations are not as prominent and are characterized by two local trends of average elevations up to 5 kg/s at 05:00 and 19:00 on August 31, 2019.

Test #5 (Fig. 8) measurements were conducted in a Section 1, while Test #3 (Fig. 7) was conducted in a Section 2, that is a reason of larger and less time-variable Q_d values were obtained (downstream Section 21 catches more Q_d compare to upstream Section 2).

Test #6 was conducted on May 20, 2020 in section #1 of the Geysernaya River (Fig. 2) for 37 min (recording frequency was min^{-1}).

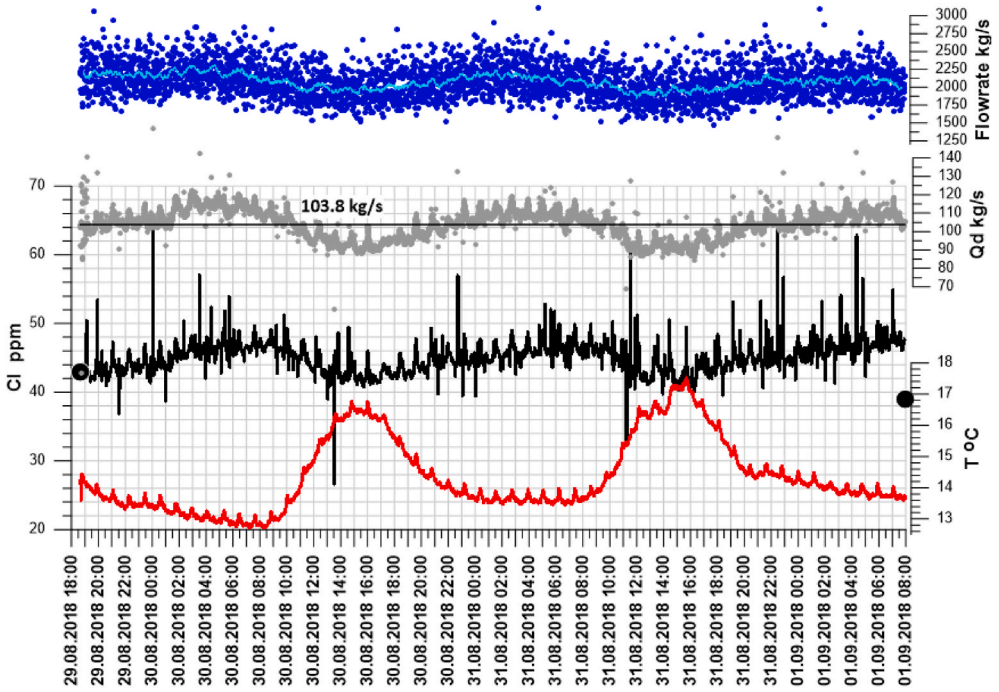

Fig. 7. Test #3: Measurements performed in section #2 of Geysernaya river (Fig. 2) during time period from August 29, 2018 to September 01, 2018. Observational data (temperature in °C and flowrate in kg/s of Geysernaya river) and output results (Cl concentrations in ppm, deep component water discharge Q_d in kg/s) are also presented in Table 1. Direct Cl sampling data are shown by black bold filled circles.

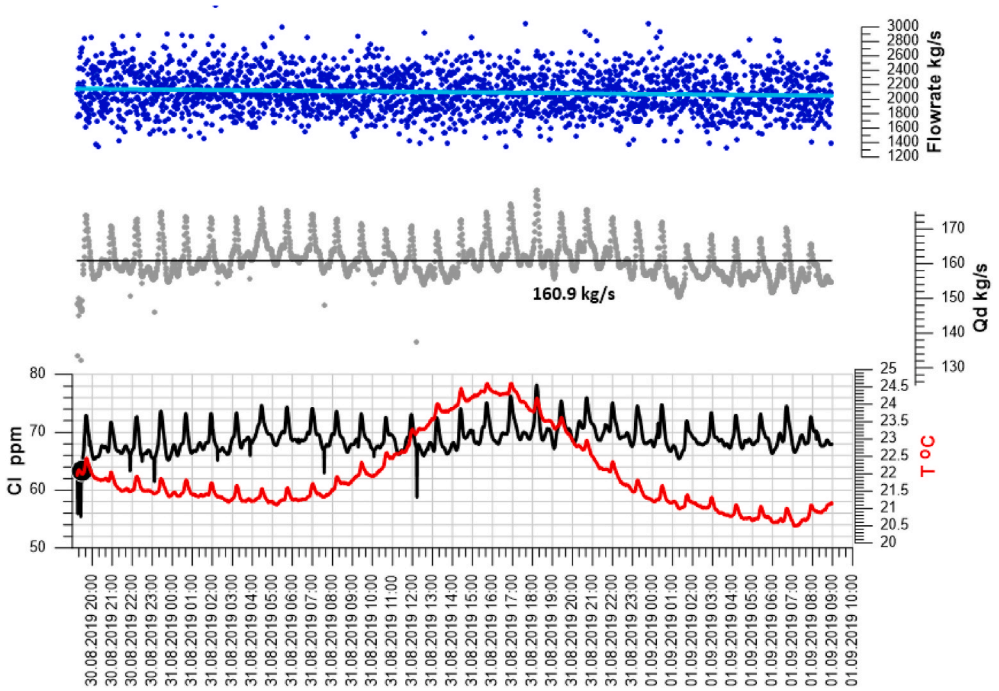

Fig. 8. Test #5: measurements performed in section #1 of Geysernaya river (Fig. 2) during the time period from August 30, 2019 to September 01, 2019. Observational data (temperature in °C, flowrate kg/s) and output results (Cl concentrations in ppm, deep component water discharge Q_d in kg/s) are also presented in Table 1. Direct Cl sampling data are shown by black bold filled circles.

Test #7 was conducted from September 08, 2020 to September 09, 2020 in Section #1 of the Geysernaya River (Fig. 2) for 19 h (recording frequency was min^{-1}).

Clear hour-cycling of chloride (specific conductance based) and temperature were observed, while the flowrate exhibited a relatively stable declining trend (Fig. 9). Very regular short-term variations were represented by 18 cycles during 19 h (corresponding to an IBE of 63 min) with temperature local maxima reaching up to 0.4–0.6 °C and chloride local maxima reaching up to 6–8 ppm. Q_d seems to have local maxima up to 7–8 kg/s, synchronized with T and Cl short-time local maximums.

Long-term Q_d variations are difficult to observe because of the short duration of testing. However, one can note the local minimum of Q_d reaching down to −5 kg/s at 02:00 on September 09, 2020.

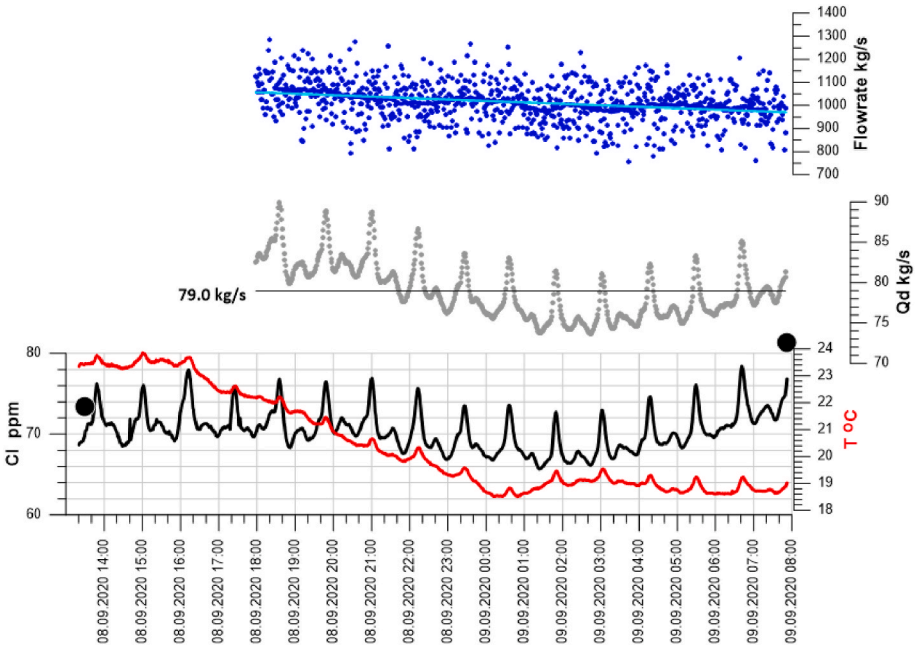

Fig. 9. Test #7: Measurements performed in section #1 of Geysernaya river (Fig. 2) from September 08, 2020 to September 09, 2020: observational data (temperature in °C, flowrate kg/s) and estimated results (Cl concentrations in ppm, deep component water discharge Q_d in kg/s) are also presented in Table 1. Direct Cl sampling data are shown by black bold filled circles.

5.2. Long term Q_d measurements (tests #LT1 and #LT2)

Long-term testing (from 108 to 126 days) were aimed to estimate the seasonal dynamics of deep-component water discharge Q_d.

Test #LT1 was conducted during time period from May 08, 2012 to August 24, 2012 in section #3 (Fig. 2) for 108 days with a set of interval measurements of 20 min, and the results are briefly described in (Kiryukhin et al., 2015). Now it is suggested to revise the past data, keeping in mind that Velikan geyser was at its full potential at that time (see below).

Test #LT2 was conducted from April 21, 2019 to August 25, 2019 in section #1 (Fig. 2) with a set of interval measurements of 10 min over 126 days. Observational data (temperature and flowrate) and output results (Cl concentrations, Q_d) are demonstrated in Fig. 10. We observe the following trends of Q_d (running average 25) transient change: (1) Relatively stable ≈275 kg/s from April 21 to May 5, 2019; (2) Trend of decline from 275 to 75 kg/s during spring-summer flooding from May 5 to July 28, 2019; (3) Late summer trend of rise from 75 to 175 kg/s from July 28 to August 25, 2019.

6. Interpretation and discussion of the results

6.1. Natural discharge time dependent conditions (year-cycle)

The total discharge of the deep component thermal water Q_d and chloride Q_{cl} estimates during the period from 1962 to 2020 are shown in Fig. 11. Those estimates include discreet and short-time measurements data (partially published (Kiryukhin et al., 2018) and are presented in section 5.1 above, total number of discreet measurements is 46), and long term specific conductance -flowmeter "continuous" observations (2 sets, presented in section 5.2). The average of discreet and short-time measurements of Q_d in the Geysernaya River were 282 kg/s (during time period from 1961 to 1994), 215 kg/s (from 2007 to 2013), and 230 kg/s (from 2014 to 2020) (Fig. 11). However, most of these discreet 46 measurements were taken in April–May or late July–October (Fig. 12). Thus, the summer data gap was filled based on specific conductance-flowmeter "continuous" measurements, which were performed in 2012 (one record per 20 min) (Kiryukhin et al., 2012) and 2019 (one record per 10 min). These data were converted into Q_d deep component water discharge and Q_{cl} chloride mass discharge, which demonstrates a decrease in Q_d down to 80–120 kg/s and Qcl to 0.090–0.130 kg/s, during summer flooding time (Fig. 12).

This may be interpreted as the local groundwater/Geysernaya River acting like a time-dependent boundary condition for the underlying Geyserny two-phase production reservoir: partially stopping discharge during summer flooding time. The Uzon geyser spring/summer switch, from geysering to pulse flow hot spring conditions may be noted as small-scale examples of such phenomena (Kiryukhin and Karpov, 2020).

The water cycle Q_d approximation graph in Fig. 12 may also be used for the annual mass component output estimates. Deep component water annual mass output estimate is equal to 8.63 million tons (annually averaged Q_d is 274 kg/s) and chloride annual mass output is equal to 7766 tons (annually averaged Q_{cl} is 0.247 kg/s) from this graph, having in account that 0.9 g/kg conversion coefficient was utilized between Q_{cl} and Q_d (assuming that concentration of chloride in the deep thermal water is 900 ppm).

Based on chemical geothermometers, Q_d may also be transformed to convective heat recharge by using the temperature of the reservoir (see Eq. (8) above). Maximum $T_{Na\text{-}K}$ temperature is estimated 225 °C in last years (Fig. 10 C in Kiryukhin et al., 201)8), which corresponds to enthalpy of water phase of 967 kJ/kg. Thus, annually averaged convective heat output Valley of Geysers is $CHF = h_w \bullet Q_d = 265$ MW.

6.2. Chloride tracing of the geysers erupted volumes

6.2.1. Synchronization of transient chloride concentration in a river and geysers (Bolshoy & Velikan) eruptions

The results presented above in section 5 indicate the possibility of applying a simple theory of tracer in a river (section 3.3) to estimate the volumes of geyser eruptions during observational times (short-term tests described in section 5.1, and long-term tests described in section 5.2). The major regularly cycling contributors in thermal discharge are just

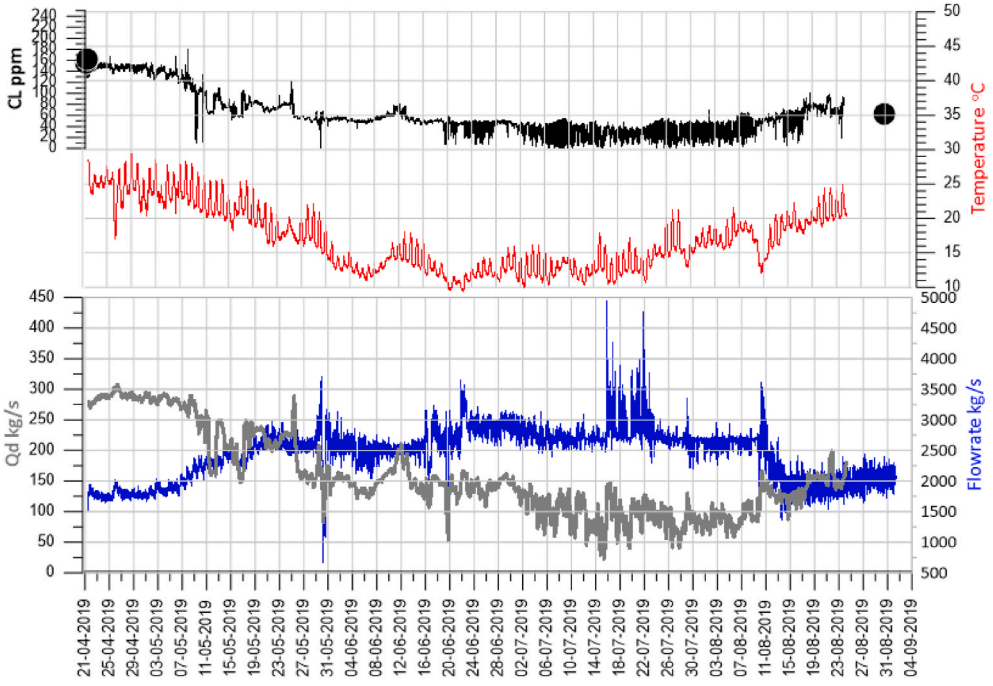

Fig. 10. Test #LT2: Measurements performed in section #1 of Geysernaya river (Fig. 2) during time period from April 21, 2019 to September 01, 2019. Observational data (temperature in °C, flowrate kg/s) and output results (Cl concentrations in ppm, deep component water discharge Q_d in kg/s) are also presented in Table 1. Direct Cl sampling data are shown by black bold filled circles. Temperature oscillations observed are daily variations of temperature.

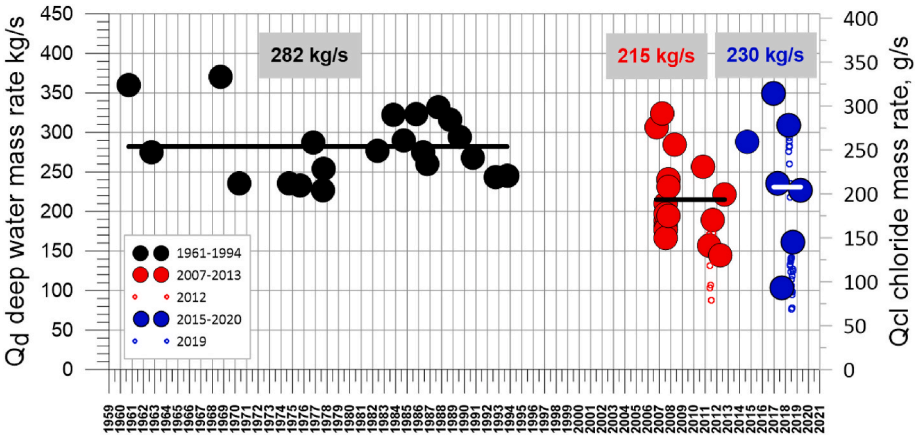

Fig. 11. Total deep component water Q_d and chloride Q_{cl} estimates from 1962 to 2020 (modified from Kiryukhin et al. (2018) with addition of new data): data from 1962 to 1994 were obtained by V.M. Sugrobov and were presented in the paper (Kiryukhin et al., 2018), data from 2007 to 2013 corresponds to section #3 measurement site, Q_d estimates based on specific conductance-flowmeter "continuous" measurements performed in 2012 and 2019 are shown by smaller circles).

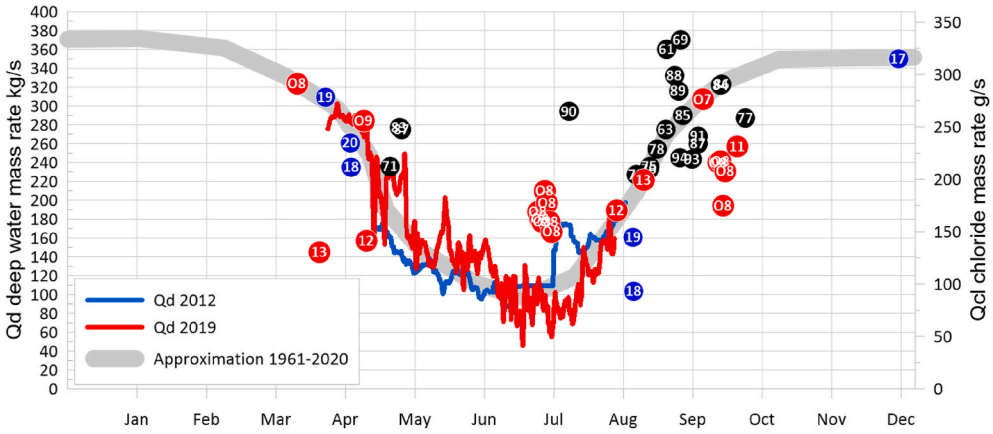

Fig. 12. Deep component water Q_d and chloride Q_{cl} during time period of hydrologic year cycle is approximated by thick gray line. Notes: (1) Input data from Fig. 11 with corresponding time period colors were used, (2) Number in a circle corresponds to year of measurements, (3) Q_d estimates based on specific conductance-flowmeter "continuous" measurements performed in 2012 and 2019 are shown by line plots. (For interpretation of the references to color in this figure legend, the reader is referred to the Web version of this article.)

two geysers, Bolshoy Geyser and Velikan Geyser, which can be seen from visual graph matches of transient chloride concentration $C_r(t)$ in the Geysernaya River and discharge temperatures $T_B(t)$ at Bolshoy and $T_V(t)$ at Velikan geysers (Figs. 13–18).

Time series cross-correlation analysis may be also used to see synchronization of parameters above mentioned. We used test #3 data for these purposes. The results of the separated cross-correlation between $C_r(t)$ - $C_b(t)$ and $T_B(t)$, $C_r(t)$ - $C_b(t)$, and $T_V(t)$ are presented in the first four columns of Table 2. The time shift in the 1-st and 3-rd columns corresponds to different travel times in minutes from geysers to the observational point (section #2 in Fig. 2), which was applied to the $C_r(t)$ - $C_b(t)$ time series. Maximum correlation coefficients of 0.162 and 0.206 were achieved for the Bolshoy geyser travel time shift of $\Delta t_B = 65$ min, and for the Velikan Geyser travel time shift of $\Delta t_V = 115$ min. Note that

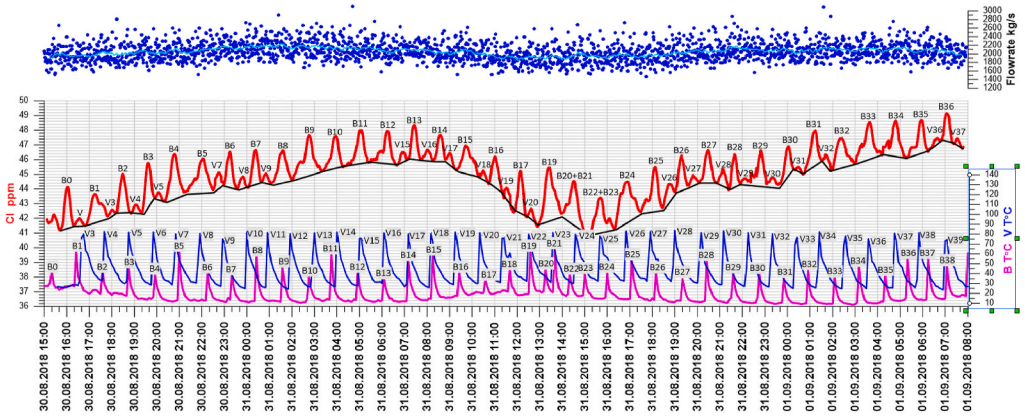

Fig. 13. Chloride inflows detected in the Geysernaya river caused by Bolshoy (B) geyser and Velikan (V) geyser eruptions activity for the time period from August 30 to September 1, 2018 (test #3). Transient Cl concentration in Geysernaya river is shown by red line (running average 31). The maximums correspond to chloride fluid eruptions from Bolshoy (B) geyser and Velikan (V) geyser at arrival times. Bottom black line is restricted to polygons, which is used for $\int C(t)dt$ calculations (see Table 3). Bolshoy (B) and Velikan (V) geysers eruption activity is expressed by temperature records collected at geyser discharge channels (B - magenta line, V – blue line). Geysernaya river flowrate is shown above. (For interpretation of the references to color in this figure legend, the reader is referred to the Web version of this article.)

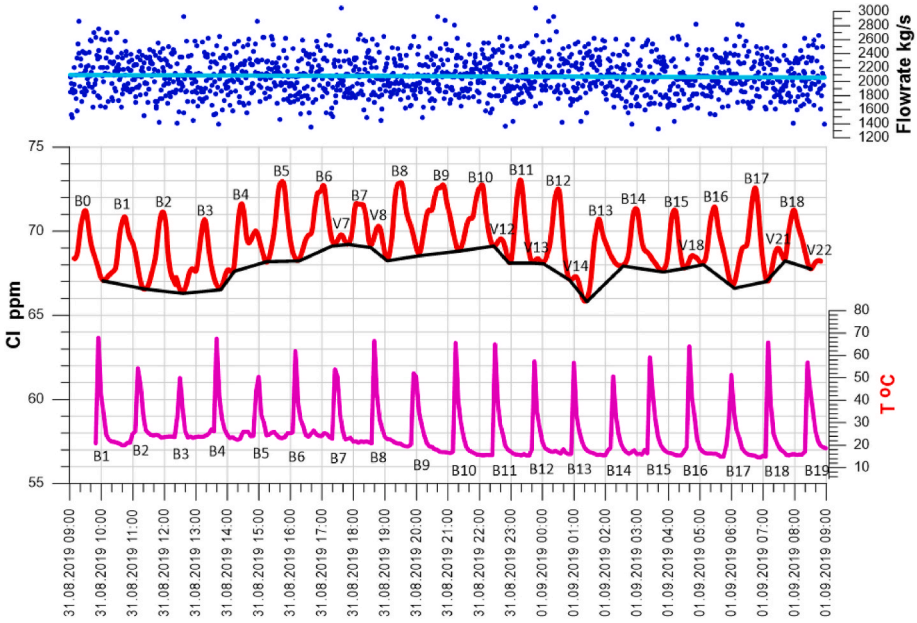

Fig. 14. Chloride inflows detected in the Geysernaya river caused by Bolshoy (B) geyser and Velikan (V) geyser eruptions activity for time period from August 31 to September 1, 2019 (Test 5). Transient Cl concentration in Geysernaya river is shown by red line (running average 17). The maximums correspond to chloride fluid eruptions from Bolshoy (B) geyser and Velikan (V) geyser arrival times. The bottom black line is restricted polygons, which are used for ∫C(t)dt calculations (see Table 3). Bolshoy (B) geyser eruption activity is expressed by temperature records collected at geysers discharge channels (B - magenta line). Geysernay river flowrate is shown above. (For interpretation of the references to color in this figure legend, the reader is referred to the Web version of this article.)

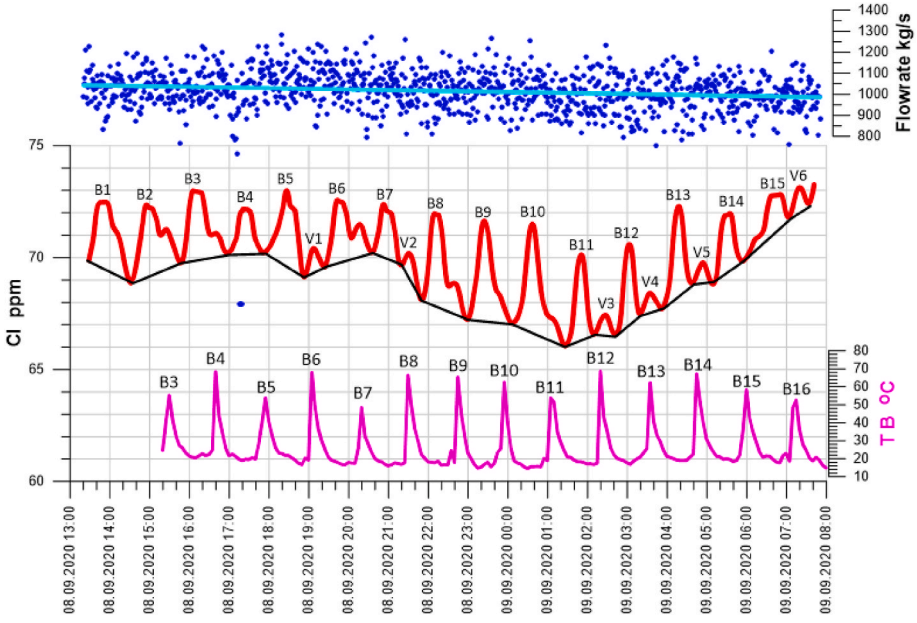

Fig. 15. Chloride inflows detected in the Geysernaya river caused by Bolshoy (B) geyser and Velikan (V) geyser eruptions activity for the time period from September 08–09, 2020 (Test 7). Transient Cl concentration in Geysernaya river is shown by red line (running average 17). The maximums correspond to chloride fluid eruptions from Bolshoy (B) geyser and Velikan (V) geyser arrival times, and the bottom black line is restricted polygons, which are used for ∫C(t)dt calculations (see Table 3). Bolshoy (B) geyser eruption activity is expressed by temperature records collected at geysers discharge channels (B - magenta line). Geysernaya river flowrate is shown above. (For interpretation of the references to color in this figure legend, the reader is referred to the Web version of this article.)

this is in good agreement with the visual graphic estimates in Table 3: 72 min and 124 min, respectively.

We can increase correlation coefficient up to 0.262, if we combine the Bolshoy and Velikan geysers normalized shifted discharge temperatures in a linear form of $\alpha \cdot T_B\,(t-\Delta t_B)+(1-\alpha)\cdot T_V\,(t-\Delta t_V)$ and use α as an adjusting parameter (see columns 5 and 6 in Table 2). This is qualitatively confirmed the Bolshoy and Velikan geysers as the main short-term (1 h) regularly cycling contributors.

The thermal slugs travelling in Geysernaya river from geysers eruptions are also clearly seen from images obtained during helicopter infrared survey (Appendix 1, Photo 9).

Thus, chloride signatures in the form of chloride transient concentration plots in Geysernaya river were used to estimate the geyser-erupted volumes according to Eqs. (10) and (11), section 3.3.

6.2.2. *Test #3 geysers erupted volumes estimates*

In Table 3, we summarize the chloride mass outputs and volumes of eruption estimates for Geysers Velikan and Bolshoy for the time period from August 30 to September 1, 2018, calculated using Eqs. (10-11), and the corresponding chloride maximum polygon area data shown in Fig. 13. Volumes of the maximum Bolshoy geyser eruptions at that time ranges from 5.4 to 18.8 m^3, and Velikan geyser yields ranges from 0.5 to 4.3 m^3. Estimated time shifts between eruptions and chloride max concentrations arrival at the point of measurements varied from 50 to 95 min for Bolshoy geyser and from 80 to 130 min for Velikan geyser. In some cases, there may be interference of Cl-concentration waves, which hinder the exact identification of the source of chloride eruption. In such cases, we estimated the integrated erupted chloride mass and corresponding water volumes.

The conduit volume of the Bolshoy geyser was determined using the tracer chloride method in 2018. A mass (m = 2 kg) of tracer (NaCl) was

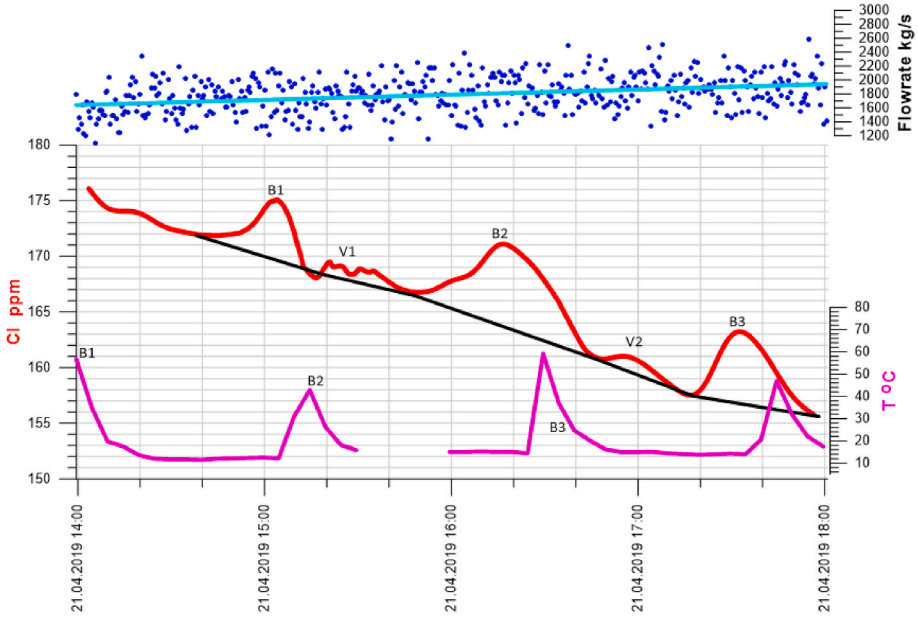

Fig. 16. Chloride inflows detected in the Geysernaya river caused by Bolshoy (B) geyser and Velikan (V) geyser eruptions activity during April 21, 2019 (Test #4). Transient Cl concentration in Geysernaya river is shown by red line (running average 17). The maximums correspond to chloride fluid eruptions from Bolshoy (B) geyser and Velikan (V) geyser arrival times, and bottom black line is restricted polygons, which is used for ∫C(t)dt calculations (see Table 3). Bolshoy (B) geyser eruption activity is expressed by temperature records collected at geysers discharge channels (magenta line). Geysernaya river flowrate is shown above. (For interpretation of the references to color in this figure legend, the reader is referred to the Web version of this article.)

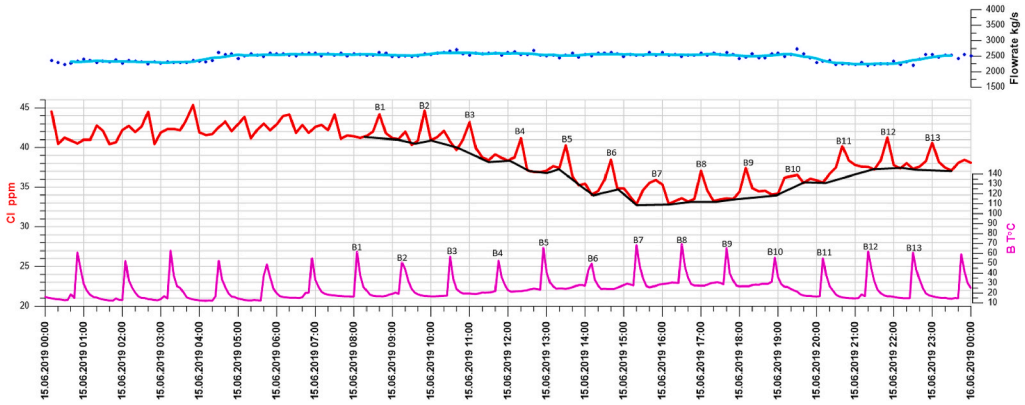

Fig. 17. Chloride inflows detected in the Geysernaya river caused by Bolshoy (B) geyser and Velikan (V) geyser eruptions activity during June 15, 2019 (Test #LT2). Transient Cl concentration in Geysernaya river is shown by red line. The maximums correspond to chloride fluid eruptions from Bolshoy (B) geyser, and the bottom black line is restricted polygons, which is used for ∫C(t)dt calculations (see Table 3). Bolshoy (B) geyser eruption activity is expressed by temperature records collected at geysers discharge channels (magenta line). Geysernaya river flowrate is shown above. (For interpretation of the references to color in this figure legend, the reader is referred to the Web version of this article.)

introduced into the Bolshoy Geyser channel before one of the eruptions (Kiryukhin, 2020, p. 162). Before tracer introduction into the geyser conduit, the chlorine ion concentration in the channel was C1 = 0.695 kg/m^3. After introduction during the subsequent eruption, the chloride ion concentration in the channel was C2 = 0.869 kg/m^3. It was assumed that the tracer (NaCl) was evenly distributed along the active conduit of the geyser. Hence, volume of active conduit can be calculated by formula V = 0.60684 m/(C2 - C1) = 3.5 m^3 (where 0.60684 is mass fraction of chlorine in NaCl). Similar volume estimate may be derived from Belousov et al. (2013). Thus, Bolshoy was able to erupt several (from 1.5 to 5.4) of its conduit volumes.

6.2.3. Test #5 geysers erupted volumes estimates

In Table 3, we summarize the chloride mass outputs and volumes of eruption estimates for Geysers Velikan and Bolshoy for the time period from August 31 to September 1, 2019, calculated using Eqs. (10) and (11) and the corresponding chloride maximum polygon area data shown in Fig. 14. Volumes of the maximum Bolshoy geyser eruptions at that time ranges from 11.9 to 28.1 m^3, and Velikan geyser yields from 0.6 to 4.5 m^3. Estimated time shifts between eruptions and chloride max concentrations arrival at the point of measurements varied from 45 to 65 min for Bolshoy geyser and from 120 to 160 min for Velikan geyser. In some cases, there is interference of concentration waves, which hinders the exact identification of the source of chloride eruption; in such cases, we estimated the integrated erupted chloride mass and the corresponding water volumes.

6.2.4. Test #7 geysers erupted volumes estimates

Table 3 summarizes the chloride mass outputs and volumes of eruption estimates for Geysers Velikan and Bolshoy for the time period from September 08 to September 09, 2020, calculated using Eqs. (10) and (11). The corresponding chloride maximum polygon area data are shown in Fig. 15. Velikan eruptions V1-V6 are clearly defined, thus we used them averaged to correct Bolshoy eruption volumes, if both eruptions were merged. Volumes of the Bolshoy geyser eruptions at that time ranges from 3.7 to 10.6 m^3, and Velikan geyser yields from 1.1 to 1.5 m^3.

6.2.5. Test #4 geysers erupted volumes estimates

In Table 3, we summarize the chloride mass outputs and volumes of eruption estimates for Geysers Velikan and Bolshoy during April 21, 2019, calculated using Eqs. (10) and (11), and the corresponding chloride maximum polygon area data shown in Fig. 16. Volumes of the maximum Bolshoy geyser eruptions at that time ranges from 12.1 to 34.6 m^3, and Velikan geyser yields from 2.9 to 3.1 m^3. The estimated

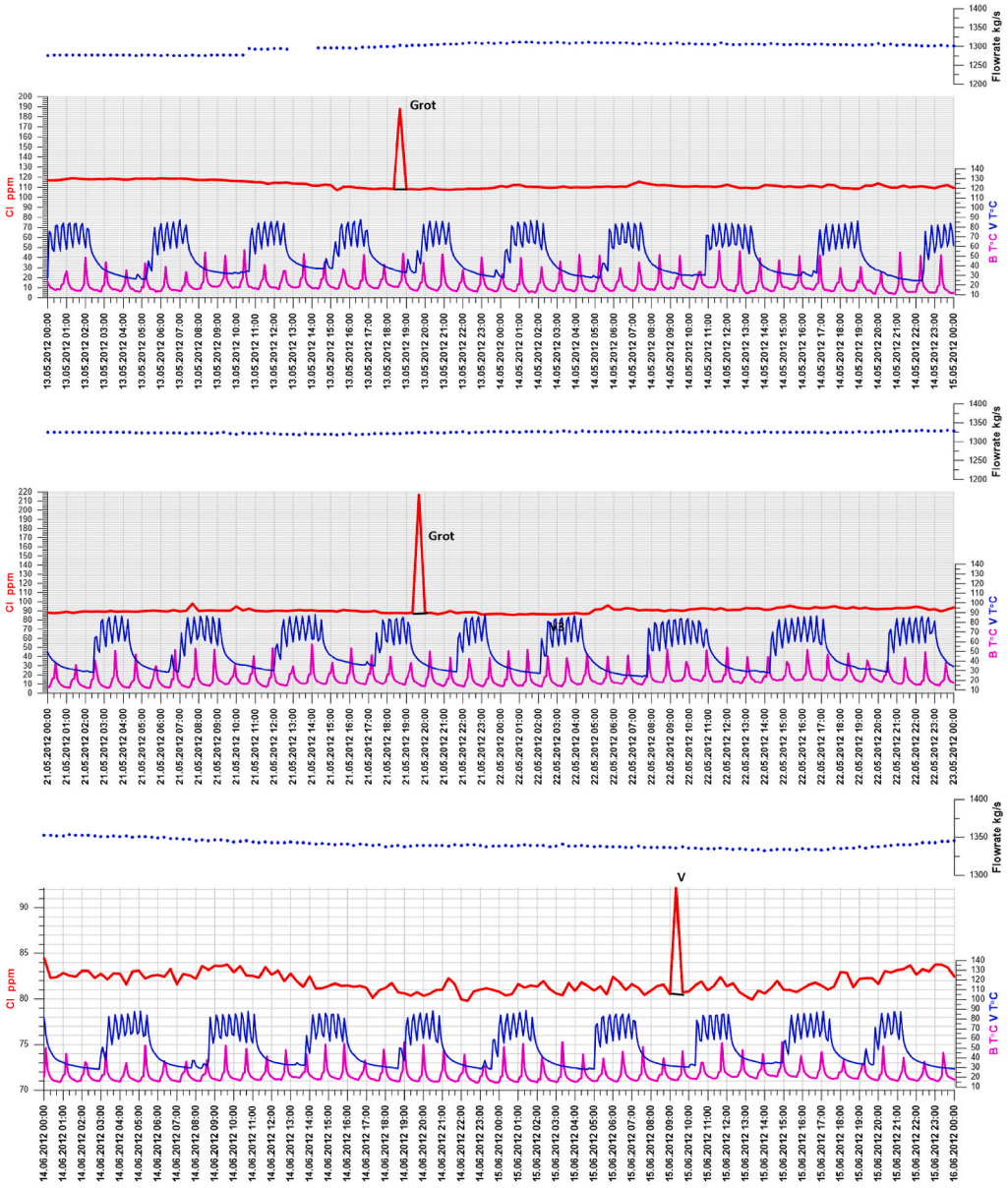

Fig. 18. Chloride inflows detected in the Geysernaya river caused by Grot and Velikan (V) geysers eruptions activity during May 13–14, May 21–22, and June 14–15, 2012 (Test #LT1). Transient Cl concentration in Geysernaya river is shown by red line. The maximums correspond to chloride fluid eruptions from Velikan (V) geyser and Grot geyser (under the Grot peak), and bottom black line restricts polygons, which were used for $\int C(t)dt$ calculations. Bolshoy (B) geyser and Velikan (V) geyser eruption activity is expressed by temperature records collected at geysers discharge channels (B - magenta line, V – blue line). Geysernaya river flowrate is shown in a curve above. (For interpretation of the references to color in this figure legend, the reader is referred to the Web version of this article.)

Table 2
Correlation coefficients R between transient chloride concentration $C(t) = C_r(t) - C_b(t)$ in Geysernaya river and discharge temperatures $T_B(t)$ at Bolshoy and $T_V(t)$ at Velikan geysers (using example of test #3). Note: Due to $Q_r(t)$ stability during time period of estimations, C (t) was used instead of $Q_{cl}(t)$.

1	2	3	4	5	6
Time shift, min	R (C & T_B)	Time shift, min	R (C & T_V)	α	R (C & $\alpha \cdot T_B + (1-\alpha) \cdot T_V$)
0	0.117	60	0.024	0	0.196
10	0.035	70	0.053	0.1	0.209
20	0.09	80	0.102	0.2	0.222
30	0.112	90	0.132	0.3	0.237
40	0.042	100	0.009	0.4	0.25
50	0.097	110	**0.206**	0.5	0.26
60	0.147	115	0.192	0.6	**0.262**
65	**0.162**	120	0.112	0.7	0.251
70	0.146	130	0.008	0.8	0.227
80	0.026			0.9	0.197
90				1	0.165

time shifts between eruptions and chloride max concentrations arriving at the point of measurements varied from 50 to 65 min for the Bolshoy geyser.

One can be seen from Table 3, that maximum volume erupted from Bolshoy geyser took place in April, that is coincide with Q_d seasonality shown in Fig. 12.

6.2.6. *Test #LT2 geysers erupted volumes estimates*

For geysers erupted volume estimations we used a single day dated June 15, 2019, from the total period of observations conducted from April 21, 2019 to August 25, 2019. Table 3 summarizes the chloride mass outputs and volumes of eruption estimates for Geysers Velikan and Bolshoy during June 15, 2019, calculated using Eqs. (10) and (11), and the corresponding chloride maximum polygon area data shown in Fig. 17. Volumes of the maximum Bolshoy Geyser eruptions in the time range from 8.6 to 23.3 m^3. The estimated time shifts between eruptions and chloride max concentrations arriving at the point of measurements varied from 30 to 40 min for the Bolshoy geyser.

Table 3
Mass of chloride and volumes of eruptions estimates for Bolshoy (B), Velikan (V) and Grot geysers for the time period from 2012 to 2019. Notes: Average chloride concentration of 780 ppm in the Velikan geyser, 700 ppm in Bolshoy geyser, and 720 ppm in the Grot geyser were used (Kiryukhin, 2020).

Test ##/Start Date	Q_r kg/s	∫C(t)dt ppm•day	M, mass of geyser eruptions kg	V, volume of geyser eruptions m^3	Geyser ## (## of eruptions)	Time shift min
#3/August 30, 2018	2061	4.0183E-02	7.134	10.2	B (33)	72
#3/August 30, 2018	2054	7.5594E-03	1.344	1.7	V (21)	124
#5/August 31, 2019	2075	8.0890E-02	14.495	19.8	B (18)	48
#5/August 31, 2019	2071	9.1433E-03	1.637	2.2	V (8)	141
#7/September 08, 2020	1011	6.4552E-02	5.656	6.8	B (15)	40
#7/September 08, 2020	1003	1.1849E-02	1.027	1.3	V (6)	
#4/April 21, 2019	1819	1.0051E-01	15.853	22.6	B (3)	58
#4/April 21, 2019	1824	1.4944E-02	2.348	3.0	V (2)	
#LT2/June 15, 2019	2483	4.2890E-02	9.152	13.1	B (13)	32
#LT1/May 25, 2012	1332	5.0694E-01	57.958	74.3	V (5)	136
#LT1/May 25, 2012	1322	1.9549E+00	223.218	310.0	Grot (2)	

6.2.7. Test #LT1 geysers erupted volumes estimates

These measurements were performed during time period from, May 08, 2012 to August 24, 2012, in section #3 (Fig. 2), as described by (Kiryukhin et al., 2015). We further used these data for Velikan geyser erupted volume estimations, which was at its full potential at that time.

Fig. 18 shows transient chloride concentrations and flowrate of the Geysernaya river during measurements conducted from May 13–14, May 21–23, and June 14–15, 2012. This figure also demonstrates erupting activity of the Velikan and the Bolshoy geysers. At that time Velikan geyser was at its full potential. Thus we believe that a large chloride maximum reflects the eruption of chloride water slugs from the Velikan at section 3 (Fig. 2), where measurements were conducted at that time. Regrettably, at that time, measurements were conducted each at 20 min, thus it was difficult to collect the Velikan eruptions entirely and precisely (which lasts just 30–40 s) in a resulting chloride curve. Thus we could identify only a few Velikan's chloride slug arrival during the period of observations from May 08, 2012 to June 15, 2012. Few of them are shown in Fig. 18, although there were more real eruptions of Velikan geyser during this time interval. We also identified arrivals of larger chloride slugs at that time period, which most probably belonged to the most powerful, but irregularly erupted Grot geyser (irregularly erupted few times in a year, video recorded on August 10, 2013).

Table 3 summarizes the chloride mass outputs and volumes of eruptions estimates for geysers Velikan and Grot during the time period from May 08, 2012 to June 15, 2012, calculated using Eqs. (10) and (11), and corresponding chloride maximums polygons area data, shown in Fig. 18. Volumes of the Velikan geyser eruptions at that time ranges from 24.0 to 144.1 m^3. The volumes of Grot geyser eruptions ranges from 289.3 to 330.8 m^3. We understand the uncertainty of this estimate due to low frequency of measurements. However, this matches closely to Velikan geyser conduit volume estimate (Kiryukhin, 2016). Estimated time shift between the Velikan eruption and the chloride max concentrations arrival at the point of measurements varies from 100 to 130 min.

Earlier, Grot geyser eruption was recorded on a video on August 10, 2013. It was impressive as a large volume of water erupted, which put Geysernaya river "out of banks". Temperature records near the Grot Geyser discharge channel during the time period from 2014 to 2015 displayed temperature maxima on January 14, 2014, August 16, 2014, December 20, 2014, and January 22, 2015, which may be interpreted as eruptions. Since then, no other evidence of Grot geyser eruption activity has been observed.

6.3. Comparison of the Valley of Geysers (Kamchatka) and world geysers fields discharge conditions

6.3.1. YNP upper basin geysers, IBE multi-year trends, seasonality, and erupted volume estimates

Few geysers have estimates of erupted volumes because water discharge is a challenging task to measure; however, those with estimates are: 8–11 m^3 during major eruptions at Lone Star (Karlstrom et al., 2013); uncertain estimates of 38–45 m^3 (Allen and Day, 1935) and 14–32 m^3 for Old Faithful (Kieffer, 1984); and 31–38 m^3 for Echinus in the Norris Geyser Basin (Clor et al., 2007).

Statistical analysis (Hurwitz et al., 2008) based on T-series cross-correlations (Madison river vs Old Faithful, Daisy, Aurum, and Depression geysers in 1996–2006) indicates negative coefficients of cross correlation (from −0.98 to −0.30) between multiyear river discharge and geyser IBE; that is, in years with high precipitation, the IBE is more frequent. In contrast, the same analysis applied to seasonality (monthly averaged IBE and river discharge in 2003–2006) yielded positive coefficients of cross correlation (from 0.7 to 0.88) and phase shift (time lags) from 2- to 6-month IBE lags. This means IBE is lengthening several months after flooding time. This is explained by the interplay of recharge/discharge boundary conditions in geyser reservoirs: more recharge runs geysers faster, while more cold-water inflows in the discharge area causes lengthening of geysers cycling. Moreover, an extended period of drought in the region should result in the IBE cessation of geysering (Hurwitz et al., 2020).

Another issue is the significant decline in the Cl mass rate during spring snowmelt (May–July 2011) observed in the main geyser discharge basin of the Firehole River (see above, McCleskey et al., 2012). This infers that the deep-component thermal water discharge rate Q_d decreases simultaneously. At that time, no phase shift (time lags) of Cl mass rate minimum vs. river discharge maximum was observed. One possible explanation is that some of the thermal features stop discharging and are converted into cold water inflow conduits during flooding times, while geysers with conduits isolated from river/ground water inflows continue regular cycling.

6.3.2. YNP Norris Geyser Basin, steamboat geyser erupted volume estimates (Reed et al., 2021)

Stream-discharge measurements from Tantalus Creek within the Norris Geyser Basin were used to estimate the Steamboat eruption volumes. For the 59 eruptions with available meteorological data and appropriate streamflow conditions for volume estimation, a negative correlation was observed between the wind speed and the volume of water discharged. This implies that stronger winds diverted some erupted water away from the established run-off channels. For the erupted volume calculations, only 29 eruptions that occurred when wind speeds were $\leq$1 m/s were used. The volumes ranged from 134 to 538 m^3, with a median of 351 m^3. No relationship between erupted volume and IBE was observed at Steamboat. In addition, there was no relationship between eruption volume and air temperature, air pressure, or amplitude of ground motion.

6.3.3. Strokkur geyser in Iceland (Eibl et al., 2020)

Strokkur is a pool geyser with a silica sinter edifice with a water basin on top. The pool is approximately 12 m in diameter with a central tube of about 2 m diameter and over 20 m depth, changing shape and temperature at 10–15 m depth. The geyser was penetrated by drillholes in

1963, as it is the most active geyser in Iceland. It is filled with hot water that is constantly around its boiling point and wobbles between the eruptions until the geyser erupts in a 30 m high water column. A local broadband seismic network for 1 year at Strokkur Geyser, Iceland, was installed which developed an unprecedented catalog of 73,466 eruptions. However, no information is available on the seasonality and eruption volumes of the Strokkur geyser.

6.3.4. El Tatio geysers multi-year trends and erupted volume estimates

The El Tatio geyser field is located north of Chile at an elevation of 4.2–4.3 km above sea level, where the temperature of boiling water is approximately 86.6 °C. El Tatio includes more than 80 active geysers. The El Jefe geyser has an eruption volume of 0.1 m^3 (110 kg (Munoz--Saez et al., JVGR, 2015a). In the EJ geyser, a difference of ~20% was observed in the IBE from 2012 to 2014 (IBE declined from 132 s to 105 s) that was not associated with changes in recharge, but instead may be caused by changes in the supply of heat, changes in the bubble trap, or changes in the permeability of the surroundings (Munoz-Saez et al., JGR, 2015b). Using the chloride inventory method, the total deep component thermal water discharge Q_d was estimated to be from 218 to 234 L/s (October 2014) (Munoz-Saez et al., JVGR, 2018). There is no information available on the multi-year trends or seasonal thermal water discharge.

6.3.5. New Zealand geysers monitoring experience

New Zealand's experience with geysers and water level monitoring for the exploitation of Whakarewarewa-Rotorua shows its possibility to identify periodic variations for both anthropogenic and barometric disturbance in the range of 2.8–5.2 mm-H2O, when the Earth tidal amplitudes are less than 1 mm-H2O (Leaver and Unsworth, 2007).

The Waimangu Volcanic Rift Valley is a hydrothermal system created on June 10, 1886, by the volcanic eruption of Mount Tarawera on the North Island of New Zealand. Echo Crater, the largest crater in the area, is filled with the steaming-hot Frying Pan Lake, which is the largest hot water spring in the world. The lake has an average depth of 6 m and covers 38,000 square meters. The average temperature of its acidic (pH 3.5) water is 55 °C, and the lake's overflow is the source of Waimangu Stream (hot water creek) flowing through the valley and into the Lake Rotomahana. Immediately, east of Echo Crater is the site of the extinct Waimangu Geyser. The crater area continued to be the source of eruptions in 1915, 1917, and last in 1973, and is still highly active. Nevertheless, there is no information available on the volumes erupted from geysers, multi-year trends or seasonality of the IBE and thermal water discharge of geysers.

6.3.6. Geysers examples in Japan

In Japan, there are many hot springs that are more than 3000, but the number of geysers are limited. #1 The Rausu-Yunosawa geyser is located inside the World Natural Heritage site of Shiretoko, Hokkaido. Once the geyser stopped, but it restarted again in 2010. #2 The Noboribetsu-Sengen geyser shows a long duration of eruption, which is longer than 50 min, and the total discharge is over 2000 L per eruption event. #3 The Shikabe Geyser, located in southern Hokkaido, was discovered through the development of hot springs in 1952 Ohtani (1961). #4 denotes two geysers, one is Benten and the other is Unryu. Benten was higher than that of Unryu. The effusion mechanism of the Onikobe geyser is boiling due to depressurization, and the geyser occasionally exhibits unstable characteristics in terms of fluctuating duration and interval times for eruption events (Nishimura et al., 2006). #5 The Kawamata geyser is located in the Kinugawa River in the Kawamata hot spring area, and the activity of the geyser became weak after 2019. #6 The Suwa Geyser was developed during hot spring drilling in 1983. In the first stage, the height was 50 m, and the activity of the geyser was weak. At a moment, artificial support was needed for eruption, so we could fix the eruption time, which is five times in a day. The first description of #7, the Atami Ohyu geyser, was recorded at 713. The eruption usually occurred five times per day (Honda and Terada, 1906), and then the activity became weak; however, the geyser was reactivated before and after the Kanto Great Earthquake in 1923 (Iwasaki, 1975). A final natural eruption was observed in 1925. Currently, artificial power is required for eruption. #8 The Kibedani Matsunoyu geyser is a low-temperature (20–21 °C) hot spring, and its mechanisms are unique. Carbon dioxide gas was emitted from a carbonate hot spring (~25 °C) and was stored beneath the subsurface water table, and then exploded a mixture of carbonate hot springs and fresh subsurface water as a geyser (Kagami, 2006). #9 Beppe is a huge hot spring area, and Tatsumaki Jigoku is a strong hydrothermal manifestation. Additionally, there are many hydrothermal explosions, including mud volcanoes, hot spring areas, and geothermal fields in Japan.

6.3.7. Valley of Geysers matches to worldwide geysers fields experience

World geysers discharge monitoring experience reveals a few examples when Q_d seasonality and geysers erupted volumes estimates were performed. Most of such kind of data came from YNP (USA), which shows indications of deep component thermal water discharge Q_d decline during flooding in Upper Geyser Basin (Fig. 12C in McCleskey et al., 2012) and geysers ability to erupt of tens or even hundreds of m^3 of water (Reed et al., 2021). This matches with observational data obtained in Valley of Geysers, Kamchatka (Russia). In spite of Iceland, New Zealand, Chile and Japan have geysers too, there was no comparable studies of transient discharge conditions of their geysers-hosted hydrothermal systems.

In terms of Q_d, Yellowstone Upper Basin (from 1200 to 1400 kg/s) is the most powerful, YNP follows by Valley of Geysers (Kamchatka) with average Q_d from 230 to 280 kg/s and El Tatio with Q_d from 218 to 232 kg/s. Yellowstone geysers shows ability to erupt of tens or even hundreds (up to 538 m^3, Steamboat geyser) of m^3 of water, that is comparable to Grot (310 m^3), Velikan (74.1 m^3) and Bolshoy (22.6 m^3) geysers in Valley of Geysers in their best times. A smaller erupted volumes were recorded in Japan (2 m^3, Noboribetsu-Sengen geyser) and in El Tatio, Chile (0.1 m^3, El Jefe geyser).

A common feature of geysers IBE seasonality, when pool type geysers IBE lengthening in winter or storm time (Daisy, Velikan) and cone type geysers IBE lengthening in summer time (Old Faithful, Bolshoy) was revealed in YNP and Valley of Geysers correspondingly.

A logic reason of seasonal flooding-related drop of Q_d observed (Yellowstone Upper Basin, Valley of Geysers) is that some of geysers and boiling springs stop their discharge activity in a flooding time. Potential candidates for this stop of deliverability in Valley of Geysers are all geysers buried by landslide of June 03, 2007 (Fig. 2C, ##5,6,30,31,34,36,38) and eroded by mudflow of January 03, 2014 along Geysernaya river. Mechanisms of this is a flooding water level rise in alluvial-clastic deposits under the Geysernaya river, which may either block discharge by pressure rise, or condensate gas phase in geyser reservoir and switch geysers channels from outflow discharge to downflow recharge BC (boundary conditions). El Chichon hydrothermal system (Mexico) also has some kind of a geyser - a boiling pulsing spring inside the crater with a similar response on the top BC: it stops when the crater lake level is high (Taran and Peiffer, 2009). Further TOUGH2-modeling may be used to explain these phenomena in required details.

Time-dependent outflow/inflow top BC impact on the Kamchatka production geothermal reservoir pressure and well production rates in the flooding period too. The Paratunsky low-temperature liquid production reservoir shows up to 0.8 bar pressure rise in a flooding time of snow melting in April–May as a response to simultaneous ground water level build atop the production reservoir (Fig. 11 in Kiryukhin et al., 2017). In contrast, the Mutnovsky high-temperature two-phase reservoir demonstrated of 2 bar pressure drop in May (well #30, 1996 year, before exploitation started, Fig. 5 in Kiryukhin et al., 2018). This shows vulnerability of geysers reservoirs (that's are in two-phase conditions) to top transient BC.

A close issue to seasonality on top boundary conditions (BC) is a cold water down-flow breakthrough during exploitation of geothermal reservoirs. Exchange of information between case histories of production geothermal fields and natural histories of geysers/boiling springs fields may benefit either geothermal industry sustainability and tourist's safety operations.

7. Conclusions

Sixty years of observations (1961–2020 years) of the deep component water natural discharge Q_d (defined using chloride discharge rate Q_{cl} in a Geysernaya River) in the Valley of Geysers hydrothermal system (Kamchatka) shows average values from 282 kg/s (during time period from 1961 to 1984) to 230 kg/s (after 2015). Extending measurements into the flooding time period (since 2012) reveals the seasonal sensitivity of Q_d: winter-frozen time discharge increases (up to 340–370 kg/s), and summer-flooded time discharge decreases (down to 100–120 kg/s). Annually averaged Q_d is 274 kg/s, Q_{cl} is 0.247 kg/s and heat flowrate recharge is 265 MW. Nevertheless, individual geyser features (cone or pool type) may cause either positive IBE sensitivity (Bolshoy, cone) or negative IBE sensitivity (Velikan, pool) to flood time periods.

More frequent observations started from 2017 (flowrate and specific electro-conductance, 1 min^{-1}) revealed short-term (about 1 h) cycling of natural discharge Q_d synchronized to internal cycling of Bolshoy and Velikan geysers, with IBEs from 60 to 75 min. This open possibility to apply a tracer chloride method to estimate the volumes of hot water erupted from the geysers. Bolshoy geyser cyclically erupted from 5 to 34 m^3, Velikan geyser cyclically erupted from 0.5 to 4.5 m^3 of hot water during time of observations from 2018 to 2020. Before the mud-flow 2014 disaster, the Velikan Geyser erupted from 24.0 to 144.1 m^3, and the Grot geyser erupted from 289.3 to 330.8 m^3 of hot water volumes, according to observations performed in 2012.

The decline of natural discharge during flooding time may be conceptually explained in terms of groundwater-river/two-phase geothermal reservoir interaction. Low or frozen water time periods restrict local infiltration of cold water from the Geysernaya River into Geyser two-phase geothermal reservoir, which benefits thermal water discharge conditions. Flood water time periods induce cold water infiltration into two-phase Geyser geothermal reservoirs, especially if gas phase condensation induces vacuum conditions, which may shut down or decline some local thermal feature discharges.

Using a conductivity method to continuously monitor the deep mass and heat flowrates recharge of Valley of Geysers hydrothermal system may be an important warning system of geological hazards (catastrophic landslides and mudflows triggered by hydrothermal discharge and explosions).

Author contributions

A.K.: conceptualization, methodology, field work, validation, data curation, writing—original draft preparation, A.P.: flowmeter data curation, N.B.: field work, data curation, N.T.: conceptualization, world geysers overview, T.R.: YNP review, IBE data validation, O.U.: YNP review, I.D.: IR data curation.

Funding

This study was funded by RFBR and JSPS according to research project # 21-55-50003.

Declaration of competing interest

The authors declare that they have no known competing financial interests or personal relationships that could have appeared to influence the work reported in this paper.

Acknowledgements

The authors express their gratitude to A.V. Sergeeva, G. Kroshkin, P. I. Shpilenok, D.M. Panicheva, R. Faizulin, A. Hachukaev, L. Podstavin, E. L. Subbotina, S.A. Chirkov for their help in field work. Authors appreciated S. Hurwitz for logistic support, Y. Taran and three unknown reviewer's for comments and suggestions, which help a lot to improve manuscript of this paper.

Appendix 1. Photos

Photo 1. Bolshoy geyser (May 2018)

Photo 2. Velikan geyser eruption before damaging by mud flow on January 03, 2014 (photo September 04, 2013, Kiryukhin A.V.).

Photo 3. Velikan geyser (photo Aug. 2018, Kiryukhin A.V.)

Photo 4A. Thermal feature "Skovorodka" (Frying pan) on a bank of Geysernaya river (30 m apart from Velikan geyser), (photo B. Uruzmetov, 2009 from Leonov, 2017, p. 281). This thermal feature was enlarged to 2 × 6 m^2 area in 2014 due to mud-flow erosion, then converted into cold water inflow recharge conditions (since 2017 year, see photo 4B)

Photo 4B. Thermal feature "Skovorodka" area was converted from boiling thermal water discharge (photo 4A) to cold water inflow recharge conditions (photo August 31, 2017, Kiryukhin A.V.).

Photo 5. New boiling fountain in place of the former boiling spring HS_Lake2 (Fig. 2) self-created in a flooding time of May 2020 (photo September 07, 2020, Kiryukhin A.V.)

Photo 6. Section #1, where chemical sampling, flowrates, water specific electro-conductance and temperature measurements were performed (photo April 21, 2019, Kiryukhin A.V.).

Photo 7. HOBO U20+U24 setup for long-term (month) before bottom installation at section #1 (photo April 21, 2019, Kiryukhin A.V.). Pair of HOBO U20 used for pressure/water level measurements, HOBO U24 was used for specific electro-conductance and temperature measurements.

Photo 8. Mainstream 400R probe setup before bottom installation in Section 1. For probe stability deployment at the bottom, an additional weight of 10.5 kg was attached.

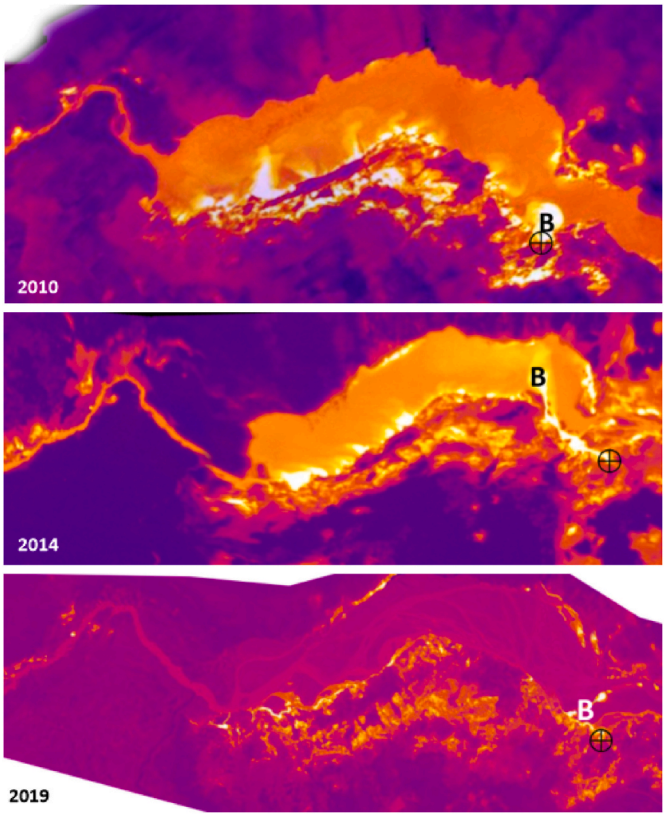

Photo 9. Helicopter infra-red surveys tracking of hot water slugs erupted from Bolshoy geyser: during discharge on August 05, 2010 (figure above), after eruption on April 28, 2014 (figure in a middle), during discharge on August 30, 2019 (figure below). Legend: B - thermal-chloride slug, crossed-circle – Bolshoy geyser location.

Appendix 2. Chloride ion concentration vs specific electro-conductance calibration

Table A2-1
Input data for chloride ion planar calibration based on Geysernaya river specific electro-conductance (SC) and temperature (T) data.

Date of sampling	SC μS/cM	T, °C	Cl ppm
24.12.17 13:08	626.0	18.4	130.0
02.05.18 11:32	886.0	25.8	170.0
29.08.18 18:39	235.2	14.1	43.0
01.09.18 7:59	248.4	13.7	39.0
21.04.19 13:44	892.8	27.6	156.0
21.04.19 18:21	795.3	25.5	163.1
30.08.19 19:30	431.0	21.0	63.4
01.05.20 12:27	972.0	28.7	166.7
08.09.20 13:30	470.1	23.4	73.4
09.09.20 7:53	437.6	19.0	81.4

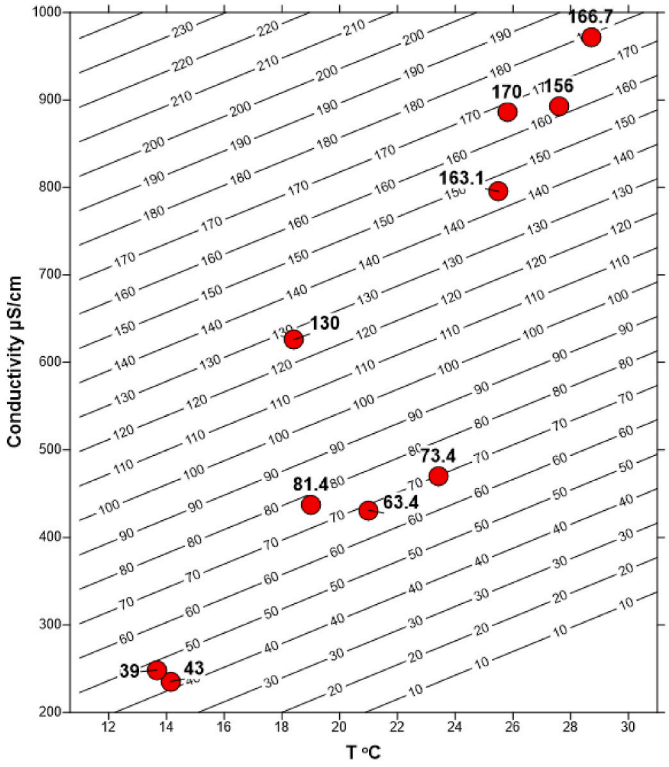

Fig. A2-1. Approximation of sampling data (Table A2-1) in a form of planar regression [Cl] = −3.461*T+ 0.254*SC+31.451

References

Allen, E.T., Day, R.L., 1935. Hot Springs of the Yellowstone National Park. Carnegie Institution of Washington, Washington, DC.

Averiev, V.V., Sugrobova, N.G., 1965. Natural Thermal Occurrences at the Pauzhetskoye Field/in the Book Pauzhetskiye Hot Waters in Kamchatka. publishing house "Nauka, Moscow, pp. 41–42 (in Russian).

Belousov, A., Belousova, M., Nechayev, A., 2013. Video observations inside conduits of erupting geysers in Kamchatka, Russia, and their geological framework: implications for the geyser mechanism. Geology 41 (3), 1–4.

Brown, P.R.L., Lawless, J.L., 1998. Characteristics of hydrothermal eruptions, with examples from New Zealand and elsewhere. Earth Sci. Rev. 52, 299–331.

Clor, L.E., Lowenstern, J.B., Heasler, H.P., 2007. "Systematics of water temperature and flow at TantalusCreek during calendar year 2005, Norris Geyser basin, Yellowstone national park, Wyoming. In: (U.S.Geological Survey Scientific Investigations Report 2007-5234. U.S. Geological Survey, Reston, VA.

Daysh, S., Carey, B., Doorman, P., Luketina, K., White, B., Zarrouk, S., 2020. New Zealand Country Update//Proceedings World Geothermal Congress 2020+1 Reykjavik, Iceland. April - October 2021.

Eibl, E.P., Hainzl, S., Vesely, N.I., Walter, T.R., Jousset, P., Hersir, G.P., Dahm, T., 2020. Eruption interval monitoring at Strokkurgeyser, Iceland. Geophys. Res. Lett. 47 (1) e2019GL085266.

Ellis, A.J., Wilson, S.H., 1955. The heat from the Weirakei-Taupo thermal region calculated from the chloride output. N. Z. For.: J. Sci. Technol. Sec. B 36, 622–631.

Fournier, R., 1989. Geochemistry and dynamics of the Yellowstone national park hydrothermal system. Annu. Rev. Earth Planet Sci. 17, 13–53.

Friedman, I., Norton, D.R., 2007. Is Yellowstone Losing its Steam?— Chloride Flux Out of Yellowstone National Park. USGS, p. 26. Professional Paper 1717.

Honda, K., Terada, T., 1906. On the geyser in Atami, Japan. Phys. Rev. XXII, 300–311.

Hurwitz, S., Lowenstern, J.B., Heasler, H., 2007. Spatial and temporal geochemical trends in the hydrothermal system of Yellowstone National Park: inferences from river solute fluxes. J. Volcanol. Geoth. Res. 162, 149–171.

Hurwitz, S., Kumar, A., Taylor, R., Heasler, H., 2008. Climate-induced variations of Geyser periodicity in Yellowstone national park,USA. Geology 36 (6), 451–454.

Hurwitz, S., Sohn, R.A., Luttrell, K., Manga, M., 2014. Triggering and modulation of geyser eruptions in Yellowstone National Park by earthquakes, earth tides, and weather. J. Geophys. Res. Solid Earth 119. https://doi.org/10.1002/2013JB010803.

Hurwitz, S., King, J.C., Pederson, G.T., Martin, J.T., Damby, D.E., Manga, M., Hungerford, J.D., Peek, S., 2020. Yellowstone's Old Faithful Geyser shut down by a severe thirteenth century drought. Geophys. Res. Lett. 47 (20) e2020GL089871.

Ingebritsen, S.E., Galloway, D.L., Colvard, E.M., Sorey, M.L., Mariner, R.H., 2001. Time-variation of hydrothermal discharge at selected sites in the Western United States: implications for monitoring. J. Volcanol. Geoth. Res. 111, 1–23.

Iwasaki, I., 1975. Geochemical indicators and seismic phenomena. Bull. Volcanol. 39, 82–90.

Kagami, H., 2006. Verification of the combined model of geyser (a periodic bubbling spring) by underground investigation of Kibedani Geyser. Adv. Geosci. 6, 203–213.

Karlstrom, L., et al., 2013. Eruptions at Lone star geyser, Yellowstone national park, USA: 1. Energeticsand eruption dynamics. J. Geophys. Res. Solid Earth 118, 4047–4062.

Kieffer, S.W., 1984. Seismicity at Old Faithful Geyser: an isolated source of geothermal noise andpossible analogue of volcanic seismicity. J. Volcanol. Geoth. Res. 22, 59–95.

Kiryukhin, A., 2016. Modeling and observations of geyser activity in relation to catastrophic landslides–mud flows (Kronotsky nature reserve, Kamchatka, Russia). J. Volcanol. Geoth. Res. 323, 129–147.

Kiryukhin, A.V., 2020. Geothermofluidomechanics of Hydrothermal, Volcanic and Hydrocarbon Systems/. Eko-Vector I-P, St. Petersburg, p. 431 (in Russian). https://elibrary.ru/download/elibrary_45739830_87259652.pdf.

Kiryukhin, A., Karpov, G., 2020. A CO2–driven gas lift mechanism in geyser cycling (Uzon caldera, Kamchatka). Geosciences 10 (5), 180. https://doi.org/10.3390/geosciences10050180.

Kiryukhin, A.V., Rychkova, T.V., Dubrovskaya, I.K., 2012. Hydrothermal system in geysers valley (Kamchatka) and triggers of the giant landslide. Appl. Geochem. J. 27, 1753–1766.

Kiryukhin, A.V., Rychkova, T.V., Dubinina, E.O., 2015. Analysis of hydrothermal regime of the Valley of Geysers (Kronotsky nature reserve, Kamchatka) after the disaster of 3.06.2007. Volcanol. Seismol. 1, 3–20.

Kiryukhin, A.V., Vorozheikina, L.A., Voronin, P.O., Kiryukhin, P.A., 2017. Thermal-Permeability structure and recharge conditions of the low temperature Paratunsky geothermal reservoirs,Kamchatka, Russia. Geothermics 70, 47–61.

Kiryukhin, A., Sugrobov, V., Sonnenthal, E., 2018. Geysers valley CO_2 cycling geological engine (Kamchatka, Russia). Geofluids J. 17. https://www.hindawi.com/journals/geofluids/aip/1963618/.

Kiryukhin, A.V., Polyakov, A.Y., Usacheva, O.O., Kiryukhin, P.A., 2018. Thermal-permeability structure and recharge conditions of the Mutnovsky high temperature geothermal field (Kamchatka, Russia). J. Volcanol. Geoth. Res. 356, 36–55.

Leaver, J.D., Unsworth, C.P., 2007. Fourier analysis of short-period water level variations in the Rotorua geothermal field. N. Z. Geothermics 36, 539–557.

Leonov, A.V., 2017. Catalog of Geysers in the Kronotsky Reserve. Valley of Geysers and the Uzon Volcano Caldera: History and Modernity. Reart Publishing House LLC, Moscow, p. 384.

McCleskey, R.B., Clor, L.E., Lowenstern, J.B., Evans, W.C., Nordstrom, D.K., Heasler, H., Huebner, M.A., 2012. Solute and geothermal flux monitoring using electrical conductivity in the Madison, Firehole, and Gibbon rivers, Yellowstone National park. Appl. Geochem. 27, 2370–2381.

McCleskey, R.B., Lowenstern, J.B., Schaper, J., Nordstrom, D.K., Heasler, H.P., Mahony, D., 2016. Geothermal solute flux monitoring and the source and fate of solutes in the Snake River, Yellowstone National Park, WY. Appl. Geochem. 73, 142–156.

McCleskey, R.B., Roth, D.A., Mahony, D., et al., 2019. Sources, fate, and flux of geothermal solutes in the Yellowstone and gardner rivers, Yellowstone national park, WY. Appl. Geochem. 111, 104458.

Moore, R.D., 2005. Slug injection using salt in solution. Streamline Watershed Manag. Bull. 8 (2), 1–6.

Munoz-Saez, C., Manga, M., Hurwitz, S., Rudolph, M., 2015a. Dynamics within geyser conduits, and sensitivity to environmental perturbations: insights from a periodic Geyser in the El Tatio geyser field, Atacama Desert, Chile. J. Volcanol. Geoth. Res. 292, 41–55.

Munoz-Saez, C., Namiki, A., Manga, M., 2015b. Geyser eruption intervals and interactions: examples from El Tatio, Atacama, Chile. J. Geophys. Res.: Solid Earth 120 (11), 7490–7507.

Munoz-Saez, C., Manga, M., Hurwitz, S., 2018. Hydrothermal discharge from the El Tatio basin, atacama, Chile. J. Volcanol. Geoth. Res. 361, 25–35.

Nishimura, T., Ichihara, M., Ueki, S., 2006. Investigation of the Onikobe geyser, NE Japan, by observing the ground tilt and flow parameters. Earth Planets Space 58, e21–e24. https://doi.org/10.1186/BF03351967, 2006.

Norton, D., Friedman, I., 1991. Chloride Flux and Surface Water Discharge Out of Yellowstone National Park, 1982-1989, vol. 1959. U.S. GEOLOGICAL SURVEY BULLETIN, p. 52.

Ohtani, K., 1961. A Study on Tsurunoyu Geyser at Shikabe Hot Spring, vol. 5. Geophysical bulletin of the Hokkaido University, pp. 51–65. https://eprints.lib.hokudai.ac.jp/dspace/handle/2115/13831?locale=en&lang=en.

Pruess, K., Oldenburg, C., Moridis, G., 1999. TOUGH2 User's Guide, Version 2.0. Rep. LBNL-43134. Lawrence Berkeley Natl. Lab., Berkeley, California.

Reed, M.H., Munoz-Saez, C., Hajimirza, S., Wu, S.M., Barth, A., Girona, T., Rasht-Behesht, M., White, E.B., Karplus, M.S., Hurwitz, S., Manga, M., 2021. The 2018 reawakening and eruption dynamics of Steamboat Geyser, the world's tallest active geyser. Proc. Natl. Acad. Sci. 118 (2).

Robertson-Tait, A., Harvey, W., Hamm, S., Boyd, L., April - October 2021. The United States of America Country Update - Electric Power Generation//Proceedings World Geothermal Congress 2020+1 Reykjavik, Iceland.

Sugrobov, V.M., Sugrobova, N.G., Droznin, V.A., Karpov, G.A., Leonov, V.L., 2009. Geysers Valley – Pearl of Kamchatka. Scientific Guidebook. Kamchatpress, Petropavlovsk-Kamchatsky.

Taran, Y.A., Peiffer, L., 2009. Hydrology, hydrochemistry and geothermal potential of El Chichón volcano-hydrothermal system, Mexico. Geothermics 38 (4), 370–378.

Update

Applied Geochemistry

Volume 140, Issue , May 2022, Page

DOI: https://doi.org/10.1016/j.apgeochem.2022.105288

Applied Geochemistry 140 (2022) 105288

Contents lists available at ScienceDirect

Applied Geochemistry

journal homepage: www.elsevier.com/locate/apgeochem

Corrigendum to "Dynamics of natural discharge of the hydrothermal system and geyser eruption regime in the Valley of Geysers, Kamchatka" [Appl. Geochem. 136 (2022) 105166]

A.V. Kiryukhin [a,b,*], A.Y. Polyakov [a], N.B. Zhuravlev [a], N. Tsuchiya [c], T.V. Rychkova [a], O.O. Usacheva [a], I.K. Dubrovskaya [a]

[a] Institute of Volcanology & Seismology FEB RAS, Piip 9, Petropavlovsk-Kamchatsky, 683006, Russia
[b] Kronotsky Federal Nature Biosphere Reserve, Ryabikova 48, Elizovo, 684000, Russia
[c] Graduate School of Environmental Studies, Geomaterial and Energy Lab., Tohoku University, Sendai, 980-8579, Japan

After our paper [Appl. Geochem. 136 (2022) 105166] was published, the co-Editor-in-Chief Zimeng Wang and the handling associate editor Marcello Liotta were informed by the readership of this paper that some texts in this paper were not properly quoted.

The authors were contacted by the editors for an explanation and cooperated with the editorial investigations into this issue. In the earlier preparation of this paper, the authors failed to realize that verbatim quotation of substantial amount of texts from other's original work should be referenced more properly, although the citations were inserted in the related paragraphs.

With this corrigendum published, the authors sincerely apologize for this misconduct and the inconvenience caused to the authors of those quoted texts and readers of the journal.

The authors hereby publish the following three sections below to replace the original texts in the published paper. The key point of this correction is to clarify that those texts are other people's original work, and that the authors were quoting their previous papers.

The technical findings and conclusions of the present paper remain unchanged.

6.3.1. YNP upper basin geysers, IBE multi-year trends, seasonality, and erupted volume estimates

"Few geysers have estimates of erupted volumes because water discharge is challenging to measure, but those with estimates erupt less water: 8–11 m^3 during major eruptions at Lone Star (63); uncertain estimates of 38–45 m^3 (12) and 14–32 m^3 for Old Faithful (ref. 66, based on ref. 53); 31–38 m^3 for Echinus in Norris Geyser Basin (67)" (Reed et al., 2021, p. 7).

6.3.2 YNP Norris Geyser Basin, Steamboat geyser erupted volume estimates

Recently published paper (Reed et al., 2021) yields the following results: "We used stream-discharge measurements from Tantalus Creek within Norris Geyser Basin (Fig. 1) to estimate Steamboat eruption volumes. For the 59 eruptions with available meteorological data and appropriate streamflow conditions for volume estimation, we found a negative correlation between wind speed and the volume of water discharged (Fig. 8A). This implies that stronger winds divert some erupted water away from established runoff channels. Thus, for erupted volume calculations, we considered only 29 eruptions that occurred when wind speeds were $\leq$1 m/s (SI Appendix, Fig. S7). The volumes range from 134 to 538 m^3 with a median of 351 m^3. For comparison, also using Tantalus Creek discharge data, Friedman (55) estimated Steamboat eruption volumes of 215 m^3 (2 May 2000), 130 m^3 (26 April 2002), and 246 m^3 (13 September 2002). We found no relation between erupted volume and the interval before or after the eruption (Fig. 8 B and C), implying unsteady heat and mass flow at Steamboat. We also found no relation between eruption volume and air temperature, air pressure, or amplitude of ground motion (SI Appendix, Fig. S8)." (Reed et al., 2021, p. 5).

6.3.3 Strokkur geyser in Iceland

Recently obtained data from Iceland geyser Strokkur were published in (Eibl et al., 2020). "Strokkur is a pool geyser and has a silica sinter edifice with a water basin on top. The pool is about 12 m in diameter with a central tube (Rinehart, 1968) of about 2 m diameter and over 20 m depth, changing shape and temperature at 10–15 m depth (Walter et al., 2018). The geyser was penetrated by drillholes in 1963, since when it is the most active geyser in Iceland (Gudmundsson, 2017). It is filled with hot water that is constantly around its boiling point and wobbling between the eruptions until the geyser erupts (Rinehart, 1968) in a ~30 m high water column (for evolution of eruption see Walter et al., 2018)." (Eibl et al., 2020, p. 2) "A local broadband seismic network for 1 year at Strokkur geyser, Iceland, and developed an unprecedented catalog of 73,466 eruptions". (Eibl et al., 2020, p. 1).

DOI of original article: https://doi.org/10.1016/j.apgeochem.2021.105166.
* Corresponding author. Institute of Volcanology & Seismology FEB RAS, Piip 9, Petropavlovsk-Kamchatsky, 683006, Russia.
E-mail address: avkiryukhin2@mail.ru (A.V. Kiryukhin).

https://doi.org/10.1016/j.apgeochem.2022.105288

Available online 29 March 2022
0883-2927/